Structures 84 (2026) 111022

Contents lists available at ScienceDirect

Structures

journal homepage: www.elsevier.com/locate/structures

Experimental and numerical insights into the structural performance of self-compacted RC box girders under combined bending, shear, and torsion

Tarek F. El-Shafiey, Emad E. Etman, Ahmed M. Atta, Ahmed T. Baraghith *, Asmaa F. Edris

Structural Engineering Department, Faculty of Engineering, Tanta University, Tanta 31511, Egypt

ARTICLE INFO

Keywords:
Box girders
Combined loading
Self-compacted concrete
Torsion to shear-depth ratio Bending
Reinforcement ratio
Finite element analysis

ABSTRACT

The high moment and torsional resistance, together with cost-effectiveness, make box girders (BGs) a more and more suitable choice for reinforced concrete (RC) bridges. However, their behavior is often complicated due to the combined effects of bending, shear, and torsion induced by traffic loads. To date, limited research has focused on evaluating the complex behavior of RC box girders, particularly when Self-Compacted Reinforced Concrete (SCRC) is employed for the cause of improved workability, durability, and sustainability of such structures. Therefore, the current study conducted experimental testing (5 specimens) and numerical analysis (19 specimens) to investigate the behavior of SCRC box girders under combined loads. The effect of torsion to shear-depth ratio (T/Vd), bottom longitudinal tensile reinforcement ratio (ρ_l), transverse reinforcement ratio (ρ_t), and wall thickness to width ratio (t_w/b) was studied. The results indicated that, when combined loading was applied to SCRC box girders with a constant moment to shear-depth ratio, the following observations were obtained: (1) Increasing T/Vd from 0.18 % to 0.92 % led to decreasing the ultimate load and the associated mid-span deflection by about 40.7 % and 67.6 %, respectively, with failure governed by torsion when T/Vd $\geq$ 0.55 %; (2) since the transverse reinforcement ratio (ρ_t) varied from 0.19 % to 1.05 %, the SCRC box girders exhibited a relatively high ultimate load, while energy absorption enhanced up to a level of 60.1 %; and (3) the enhancement in the ultimate load reached about 26.0 % when the wall thickness increased by twofold.

1. Introduction

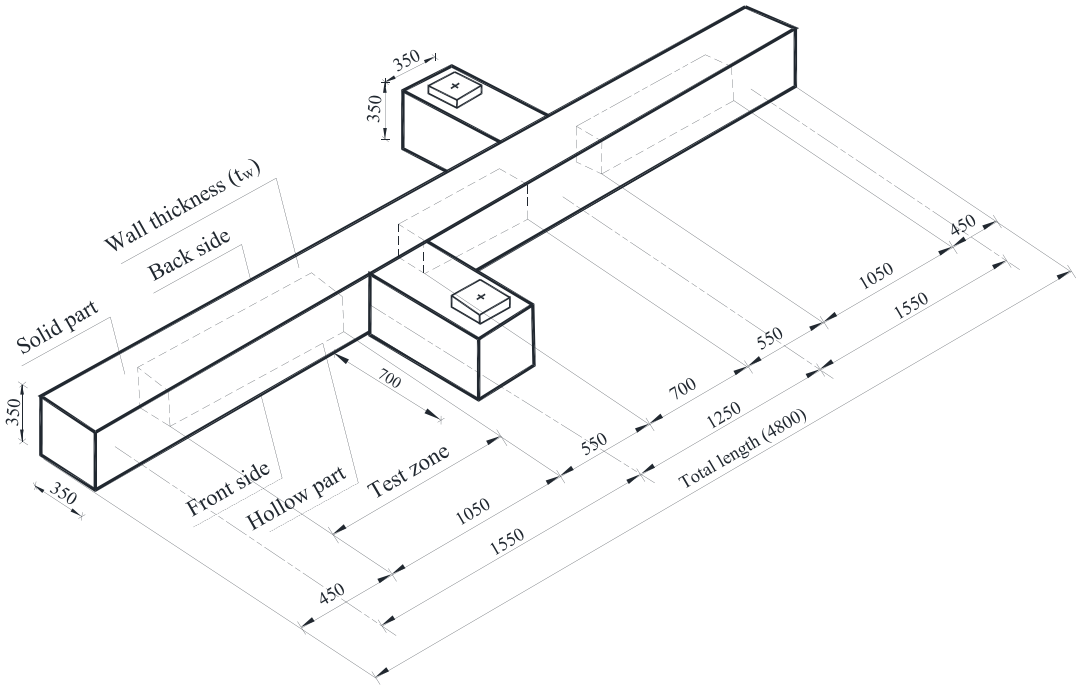
Box Girders (BGs) have gained wide acceptance in infrastructures, especially for long spans bridges, due to their remarkable flexural and torsional stiffness, as well as their excellent structural efficiency (economical construction, high stability, serviceability, and pleasing aesthetics) [1]. BGs can be categorized in so many ways according to their construction methods, use, and shape. They may be constructed as single cell, double cell, or multicell. Furthermore, their sections may be rectangular, trapezoidal, or circular [2–4]. In spite of that, box girders have thin sections, reinforcement congestion, and utilize a complex framework; such actions lead to a low compaction issue [5].

Recently, Self-Compacted Concrete (SCC) has become more popular and attracted the interest of researchers because of the rapid development in concrete technology and construction techniques towards sustainable applications [6]. SCC may be defined as an excellent workability concrete that flows under its own weight without needing any vibration for placing and compaction, compared to normal concrete [7–12]. The water-to-binder ratio in SCC is reduced by adding a minimum dosage of superplasticizers and viscosity-modifying agents [13]. In 1983, Hajime Okamura, who is known as the father of SCC technology, proposed the utilization of SCC within thin RC members, like BGs, especially in the presence of congested reinforcement, to address the issue of durability [14–15].

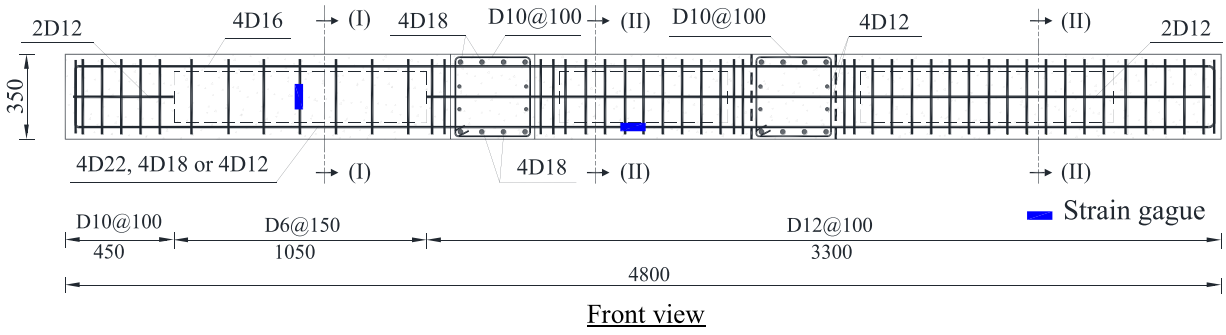
In real-world applications, box girders often experience a combined effect of bending, shear, and torsion as a result of non-uniform traffic loads, which in turn leads to complex behavior [16]. For clarification, bending moments create flexural stresses that can lead to cracking, whereas shear forces and torsional moments further complicate stress distribution [17–19]. To guarantee the integrity of the entire structure, it is crucial to understand the behavior of BGs under these combined stresses. However, to the authors' best knowledge, this interaction has not yet been fully studied, especially for BGs. Most studies are conducted on the behavior and ultimate capacity of RC members under flexure [20–30], shear [31–40], and torsion [41–48] separately, and there is no general agreement on their combined effects. Moreover, in most codes of practice [49–53], the calculation of reinforcement for each load is done individually and then summed algebraically, which leads to

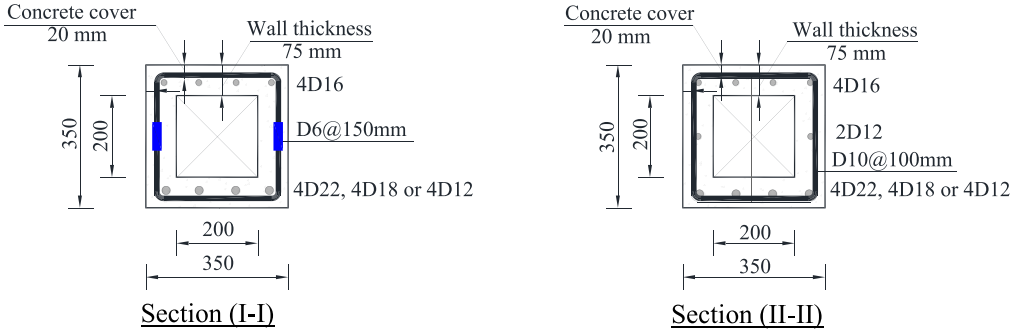
* Corresponding author.
E-mail addresses: ahmed.baraghit@f-eng.tanta.edu.eg, ahmed_baraghit@yahoo.com (A.T. Baraghith).

https://doi.org/10.1016/j.istruc.2025.111022
Received 4 September 2025; Received in revised form 26 November 2025; Accepted 24 December 2025
Available online 30 December 2025
2352-0124/© 2025 Institution of Structural Engineers. Published by Elsevier Ltd. All rights are reserved, including those for text and data mining, AI training, and similar technologies.



(a) Overall view and concrete dimensions





(b) Reinforcement details

Fig. 1. Geometry and reinforcement details of the tested box girders (all dimensions in mm).

conservative design.

Alnuaimi et al. [54] conducted an experimental program to study the effect of combined loading on hollow RC beams. According to their research, the ultimate loads were found to be inversely proportional to the torsion to bending moment ratio. MohamedSalih and Yousif [55] investigated the behavior of high strength concrete box girders subjected to combined loading. The key parameters were the cross-sectional shape (rectangular or trapezoidal), cover thickness, concrete wall thickness, and reinforcement layout. In terms of both flexural and torsional behavior, the results demonstrated that the rectangular specimen surpassed its trapezoidal counterpart. In addition, experimental and numerical investigations on reinforced Light Weight

Table 1
Tested SCRC box girders.

Specimen ID	e (mm)	T/Vd	ρ_l	ρ_t	t_w/b
BG-0.27–3.24	300	0.27	3.24	0.25	0.21
BG-0.46–3.24	500	0.46	3.24		
BG-0.64–3.24	700	0.64	3.24		
BG-0.64–2.15	700	0.64	2.15		
BG-0.64–0.95	700	0.64	0.95		

Where e = the load eccentricity from the center of the box girder; T/Vd = the torsion to shear-depth ratio; ρ_l = the bottom longitudinal tensile reinforcement ratio; ρ_t = the transverse reinforcement ratio at the test zone; t_w/b= the wall thickness to width ratio.

Foamed Concrete (LWFC) T-beams and L-beams were performed by Deifalla et al. [56–57]. It was discovered that the capacity of the LWFC beam increased in conjunction with the reduction in the torsion to shear-depth ratio.

The above-mentioned features of RC box girders open up new research opportunities, especially under the effect of combined loading, with the necessity of using SCC to realize the durability and sustainability of such elements.

2. Research significance

Reinforced concrete box girders (BGs) are important elements in infrastructure structures like concrete bridges. However, studies on how they behave under combined loads are still scarce, especially when self-compacting concrete (SCC) is utilized in order to avoid honeycombing due to the small section thickness and reinforcement congestion. It may be attributed to: (a) the specialized nature of the problem, (b) the massive experimental budgets required, (c) the difficulty in conducting realistic testing, and (d) complicated analyses. On the other hand, the international design codes do not provide any provision or limits for designing RC members under combined loading. This urges the necessity for this landmark study to advance the current understanding of SCRC box girders under combined bending, shear, and torsion, contributing to the provision of a valuable database that will open up new research opportunities to derive more accurate and relevant equations.

In light of the aforementioned challenges, this study uniquely addresses this gap by experimentally and numerically examining the behavior of self-compacted reinforced concrete (SCRC) box girders under a combined loading of bending, shear, and torsion. The experimental program included testing five SCRC box girders with different torsion to shear-depth ratios (T/Vd) and variable bottom longitudinal tensile reinforcement ratios (ρ_l). The performance was evaluated on the basis of crack pattern, failure mode, cracking and ultimate loads, deflection, angle of twist, steel reinforcement strain, and energy absorption. Furthermore, a parametric study was performed by developing and verifying an ABAQUS numerical model [58] with experimental data. Then, different ratios of torsion to shear-depth (T/Vd) and bottom longitudinal tensile reinforcement (ρ_l) had been investigated. In addition, the effect of the transverse reinforcement ratio (ρ_t) and the wall thickness to width ratio (t_w/b) was studied. Important insights into the behavior of such members can be achieved through the study findings.

3. Experimental work

3.1. Test specimens

Five identical specimens were prepared and tested to examine the impact of combined loading on the behavior of SCRC box girders. The concrete dimensions and reinforcement details of the tested specimens are illustrated in Fig. 1. The SCRC box girders were designed with a square cross-section of 350 × 350 mm and a wall thickness of 75 mm. A moderate concrete cover of 20 mm was taken based on recommendations from previous studies on box girders under combined loading [1, 59]. This concrete cover was chosen to avoid probable spall-off resulting from using large concrete covers in members that were subjected to significant torsional stresses. The total length of the box girder was 4800 mm, while the center-to-center span was 4350 mm. The critical zone, where the combined loading acts (bending, shear, and torsion), has a length of 1050 mm. It should be noted that the concrete's cross-sectional dimensions were chosen to comply with the criteria for thick-walled box girders as stated in Vlasov's theory. This is valid when one of the following conditions is satisfied: (a) the span should not be more than ten times the width or height of the member, or (b) neither the width nor the height of the member should be more than ten times the thickness of its wall. In such a way, the impacts of shear lag, distortion, and warping stresses were ignored [60].

Two transverse cantilevers (350 mm height, 350 mm width, and 700 mm clear length) were monolithically cast to convey a twisting torque without gaps and slips between the cantilevers and the specimen, thereby eliminating errors in the measurement of small deformations, as indicated in previous studies [61–64]. Four reinforced solid parts were incorporated: two 450 mm wide at each end of the box girder and two 550 mm wide at the intersection of the cantilevers with the box girder; see Fig. 1. The solid parts were used not only to counteract the effects of torsional and distortional warping constraints but also to guarantee that failure will occur inside the test zone [65]. Low-density polystyrene blocks (0.195 gm/cm^3) were used to form the specimen's hollow parts.

The tested box girders were reinforced with four deformed steel bars: 22 mm, 18 mm, or 12 mm-diameter (at the bottom) and 16 mm-diameter (at the top). Moreover, smooth bars of 6 mm-diameter closed stirrups spaced every 150 mm (D6@150 mm) were utilized in the test zone. Over the remaining span of the box girder, D12@100 mm deformed bars were used to prevent the failure occurrence outside the test zone. This reinforcement configuration was chosen based on a wide range of previous research related to the current study [66–68]. The transverse cantilevers were provided with top and bottom longitudinal reinforcement (4D18) as well as stirrups (10 mm-diameter deformed bars spaced every 100 mm); see Fig. 1.

Table 3
Properties of the steel reinforcement determined in laboratory tests.

Diameter D (mm)	Yielded strength f_y (MPa)	Ultimate strength f_u (MPa)	Yielded strain ε_y (μs)	Young's modulus E_s (GPa)
6	280	395	1400	200
10	440	625	2180	202
12	455	605	2250	202
16	430	620	2100	205
18	420	620	2060	204
22	415	610	2030	204

Table 2
Mix proportions per meter cubic of SCC materials (kg/m^3).

Concrete mix	Coarse aggregate	Sand	Cement	Silica fume	Superplasticizer	Water	W/B
SSC	900	810	400	15	8.5	185	0.45

SCC = Self-compacted concrete; W/B = the water/ binder ratio; B = cement + silica fume.

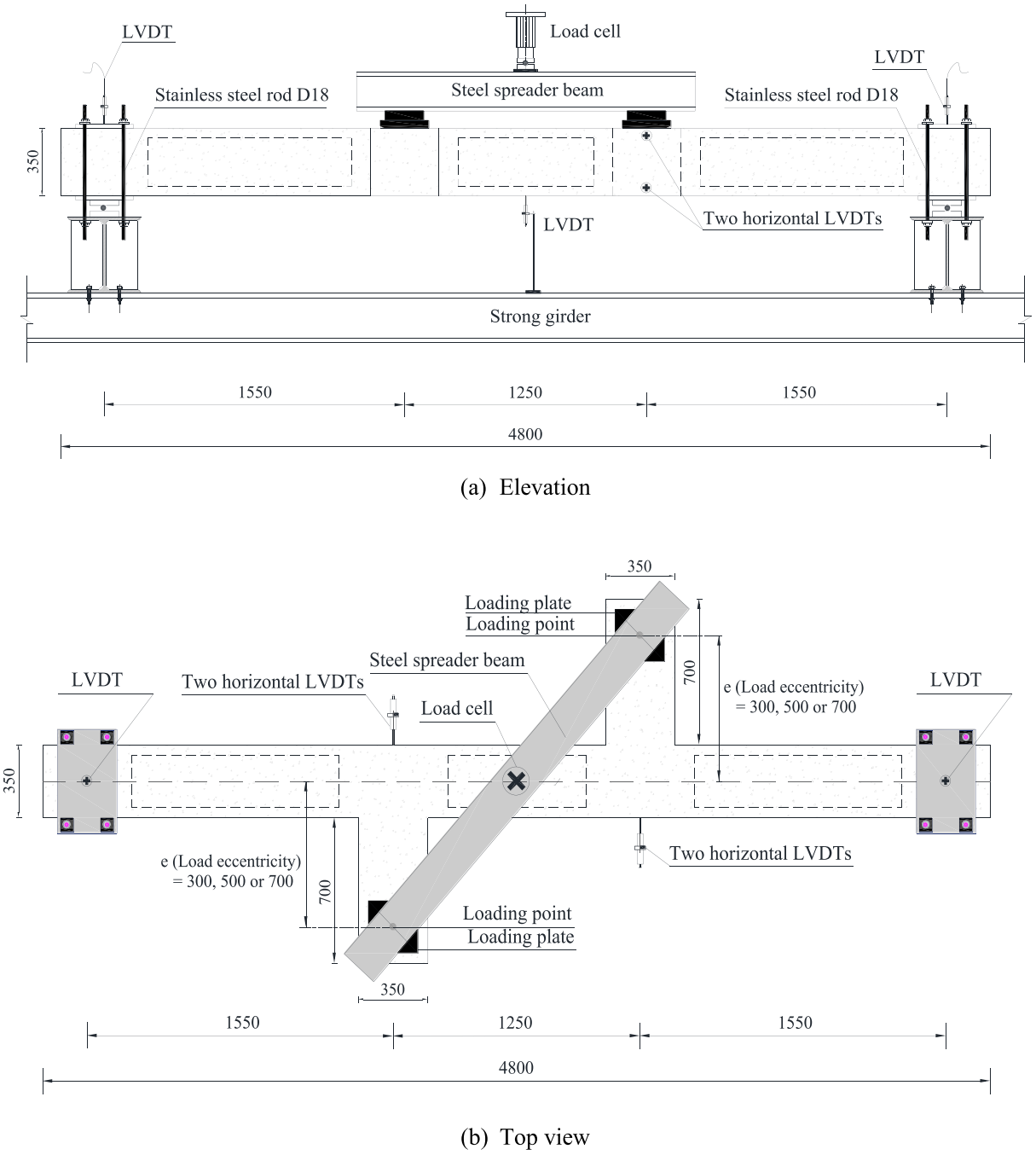


Fig. 2. General view of the test setup for a box girder (all dimensions in mm).

As shown in Table 1, two test variables were investigated in this study: (a) torsion to shear-depth (T/Vd = 0.27 %, 0.46 %, or 0.64 %); and (b) bottom longitudinal tensile reinforcement (ρ_l = 0.95 %, 2.15 %, or 3.24 %). All test box girders, merged with two cantilevers in the opposite direction, were cast in pre-prepared plywood forms. The molds were clean and strong enough in order to carry concrete weight and were sprayed with clean water before casting SCC to prevent the absorption of mixing water. The reinforcement cages were held to obtain the required covers and to avoid any displacement or floating during casting.

3.2. Material properties

In order to maintain quality control, a ready-mix self-compacted concrete (SCC) mix was provided by a local concrete supplier. SCC was chosen to facilitate pouring concrete in box girders with limited thickness and heavy reinforcement. The proportions required to produce 1 m^3 of SCC are listed in Table 2. The mix involved Ordinary Portland Cement, clean contaminant-free sand as a fine aggregate, crushed dolomite to represent the coarse aggregate, and clean tap water. To completely fill the voids inside the SCC mixture, silica fume was included as pozzolanic fillers. Also, superplasticizer was added to the SCC mixture to enhance the workability of the mix. In accordance with ASTM standard [69], all box girders were wet-sackcloth-cured for two weeks before being left to air-dry until the testing day.

The standard fresh tests of SCC were carried out to ascertain that the used mix achieved its functional requirements: (1) the slump flow test (a flowability indicator) demonstrated that the SCC circle had an average

Table 4
Experimental results for all tested SCRC box girders.

Specimen ID	Loads			Displacement			Torque			Angle of twist			Stiffness				Ultimate strains			Energy absorption
	P_{cr} (kN)	P_y (kN)	P_u (kN)	$\triangle_{cr}$ (mm)	$\triangle_y$ (mm)	$\triangle_u$ (mm)	T_{cr} (kN.m)	T_y (kN.m)	T_u (kN.m)	φ_{cr} (rad)	φ_y (rad)	φ_u (rad)	K_{flun} (kN/mm)	K_{fcr} (kN/mm)	K_{Tun} (kN.m/rad)	K_{Tcr} (kN.m/rad)	S_l (με)	S_{tf} (με)	S_{tb} (με)	E (kN.mm)
BG-0.27–3.24	120.0	259.5	291.4	10.62	30.64	64.64	5.2	11.2	12.5	0.0018	0.0094	0.0276	11.30	3.17	2889	283	1787	1640	1395	15019
BG-0.46–3.24	77.0	225.8	256.7	7.49	29.24	47.61	5.5	16.3	18.5	0.0016	0.0175	0.0447	10.28	4.48	3438	302	1751	1465	1046	9080
BG-0.64–3.24	62.0	191.6	231.2	6.33	24.68	38.72	6.2	19.2	23.1	0.0017	0.0209	0.0484	9.79	5.22	3647	362	1704	1470	381	6370
BG-0.64–2.15	63.0	162.4	187.6	6.50	25.39	44.36	6.3	16.2	18.8	0.0018	0.0169	0.0429	9.69	3.29	3500	304	2180	1486	502	6809
BG-0.64–0.95	55.0	102.6	121.5	6.81	24.38	60.09	5.5	10.3	12.2	0.0028	0.0133	0.0329	8.08	1.25	1964	223	2516	1759	605	6921

Where P_{cr} = first diagonal shear cracking load; P_y = yielding load; P_u = ultimate load; $\triangle_{cr}$ = deflection corresponding to the first diagonal shear cracking load; $\triangle_y$ = yielding deflection; $\triangle_u$= ultimate deflection; T_{cr} = cracking torque; T_y = yielding torque; T_u = ultimate torque; φ_{cr} = cracking angle of twist; φ_y = yielding angle of twist; φ_u = ultimate angle of twist; K_{flun} = uncracked flexural stiffness; K_{fcr}= cracked flexural stiffness; K_{Tun} = uncracked torsional stiffness; K_{Tcr} = cracked torsional stiffness; S_l = maximum strain in the bottom longitudinal tensile reinforcement; S_{tf} = maximum strain in the transverse reinforcement at the middle of the test zone (front side); S_{tb}= maximum strain in the transverse reinforcement at the middle of the test zone (back side); E = the energy absorption.

diameter of about 610 mm (acceptable at 600–800 mm), and the time until the SCC touched the 500 mm circle was almost 3.8 s (acceptable at 2–5 s); (2) the L-box test (a passing ability assessment) yielded the passing factor value (H2/H1) of almost 0.85, where H2 represents the height of the SCC at the end of the horizontal section, and H1 denotes the total height (the acceptable limits of H2/H1 are greater than 0.8); and (3) the V-funnel test (a segregation resistance evaluation) represented that the fresh SCC flowed through the apparatus (To) in approximately 6 s. Additionally, the time recorded for the segregation tendency of fresh SCC, which was allowed to settle for 5 min before passing via the V-funnel (T5), was approximately 9 s (acceptable at To from 6 to 12 s, and T5-To less than or equal to 3 s). As indicated, the findings of the fresh tests conducted on the used mix were consistent with several specifications for SCC [70–71].

In line with [50], the compressive strength of SCC was evaluated on the testing day using six standard cubic specimens, each with a 150 mm side length. In addition, the splitting tensile strength of SCC was determined by testing six standard cylindrical specimens (150 mm-diameter and 300 mm-height) as per the requirements of [72]. On average, the compressive strength and indirect splitting tensile strength were about 35.5 and 3.2 MPa, respectively. To assess the mechanical properties for the longitudinal steel bars and stirrups, tensile tests were performed on three typical specimens for each bar size in accordance with ASTM A615/A615M-16 [73]. The mean values of tensile yield strength, ultimate strength, and Young's modulus for each bar size are summarized in Table 3.

3.3. Test setup and instrumentation

The combined experiments, including torsion, were conducted by providing a three-dimensional working platform. An IPE 240 beam, measuring 2400 mm in length, was arranged diagonally on the top of the tested box girders. All tests were conducted at ambient temperature to exclude the damage associated with higher temperatures, such as those that occur during fire events [74–75]. The test began with a vertical load that was applied through the hydraulic jack of the loading frame to the center of the IPE. To prevent out-of-plane bending rather than twisting, it was confirmed that the plane of loading and twisting was perpendicular to the longitudinal axis of the box girders before testing. Fig. 2 presents a schematic overview of the test setup for a box girder.

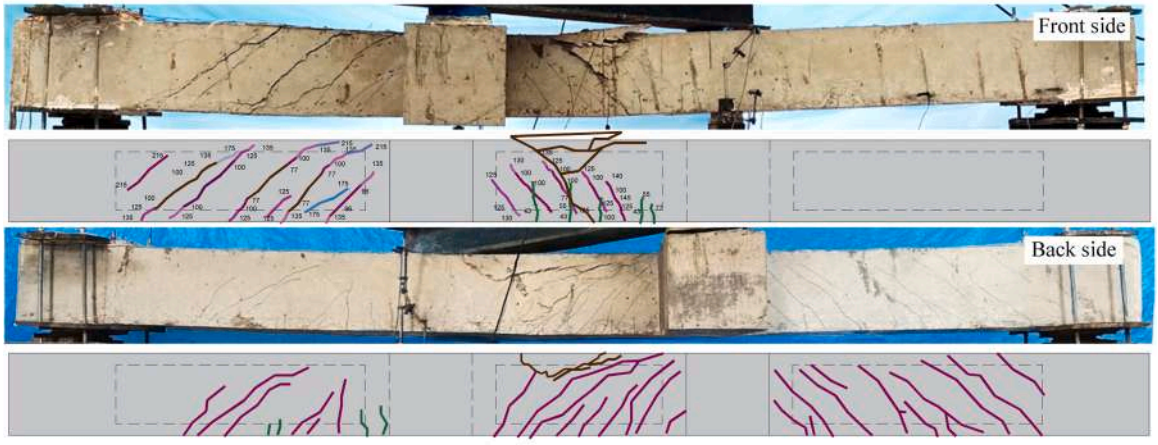
From a structural standpoint, the applied eccentric loads in the test setup were chosen to simulate and represent the actual loading scenarios for bridges, which simultaneously induce bending, shear, and torsion in a fixed-fixed box girder. Depending on the structural analysis, the test zone is most likely anticipated to experience shear-dominated failure modes. Thereby, the reinforcement steel was intensified in the whole box girder's parts except the test zone to concentrate on the combined action (bending, shear, and torsion) in this study. Otherwise, the middle zone is subjected to only bending and torsion.

Three LVDTs (100 mm gauge length) were utilized in both the mid-span and support sections to extract the net vertical deflection. The angle of twist was determined using a simple mechanical system incorporating four LVDTs. Each pair of these LVDTs was fixed horizontally, perpendicular to the side of the tested box girder, maintaining a vertical distance of 270 mm between them at the maximum expected rotation, as illustrated in Fig. 2. In addition, electrical strain gauges were fixed to both longitudinal and transverse reinforcements at pre-assigned locations to monitor the normal strains developed during the test, as depicted in Fig. 1.

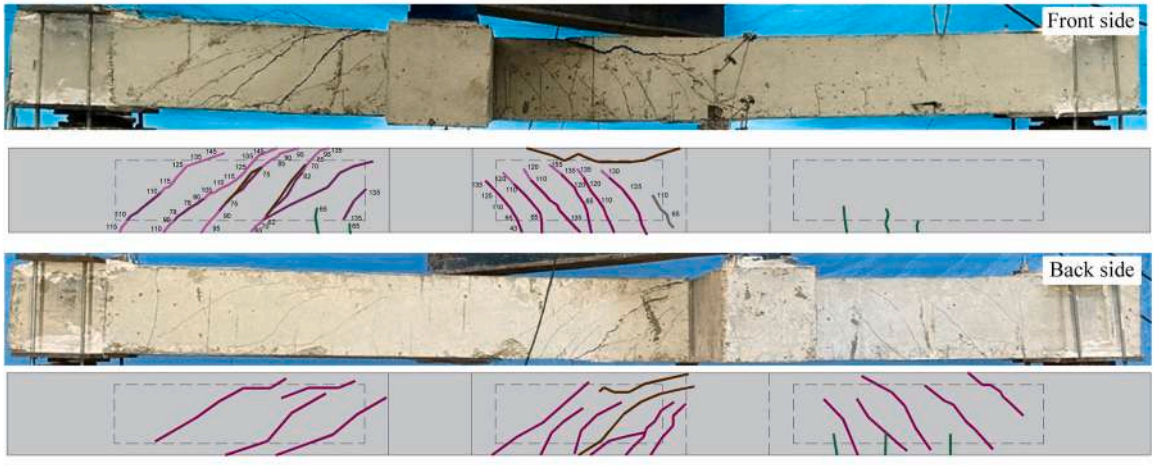
Up to failure, all tested box girders were incrementally loaded using a hydraulic jack at the loading point at intervals of about 10 kN. Following each load interval, the load was carefully maintained, and any unforeseen movements were carefully examined throughout the loading rig, while the developed cracks were marked on the concrete surface. The applied load on the tested box girder was measured by a load cell with a capacity of 1000 kN. It is worth mentioning that all LVDTs and



(a) Box girder BG-0.27-3.24



(b) Box girder BG-0.46-3.24



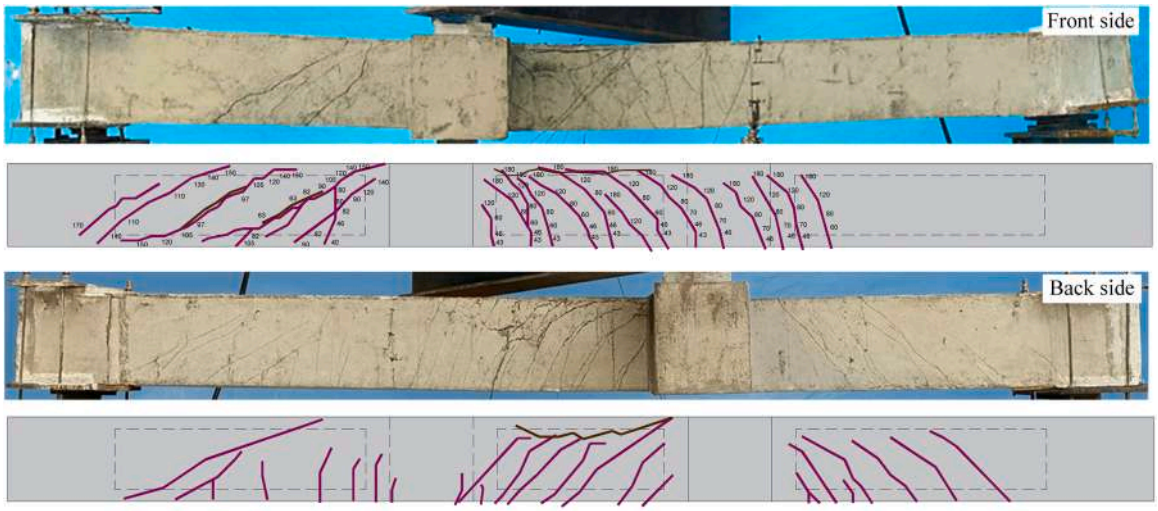
(c) Box girder BG-0.64-3.24

Fig. 3. Crack patterns at complete failure for all tested SCRC box girders.

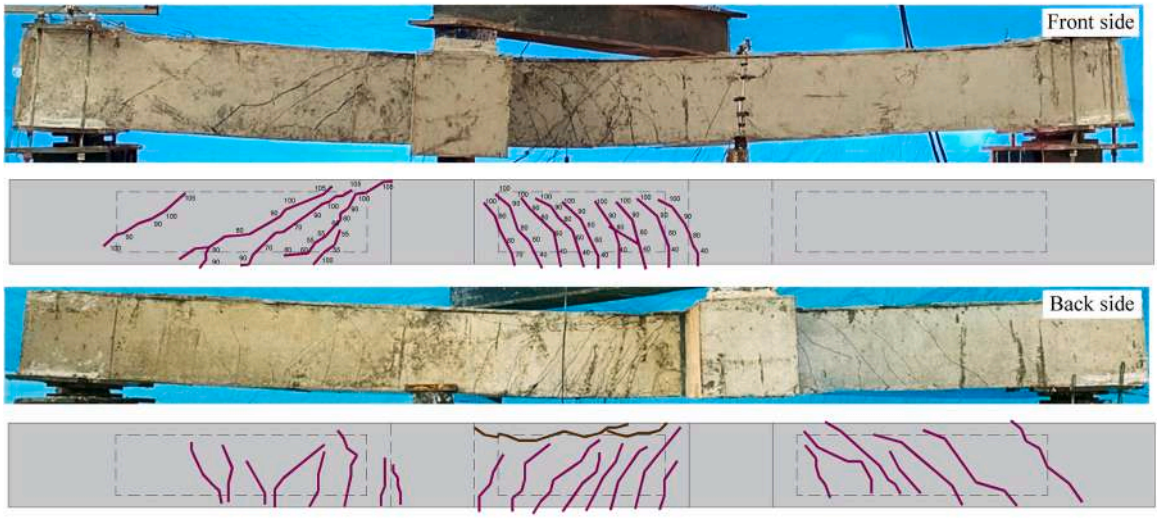
strain gauges were calibrated according to manufacturer specifications before testing to ensure accurate readings. The deflection, twists, and strain measurements were recorded and stored using a high-precision data acquisition system (KYOWA model PCD-300A with a rate of 5 kHz).

4. Experimental results and discussion

The experimental results are discussed and analyzed to assess the effects of the studied parameters on the behavior of tested SCRC box girders subjected to combined loading (bending, shear, and torsion), as detailed in Table 4. These results include the crack pattern, modes of failure, ultimate capacity, load-displacement response, torque-angle of

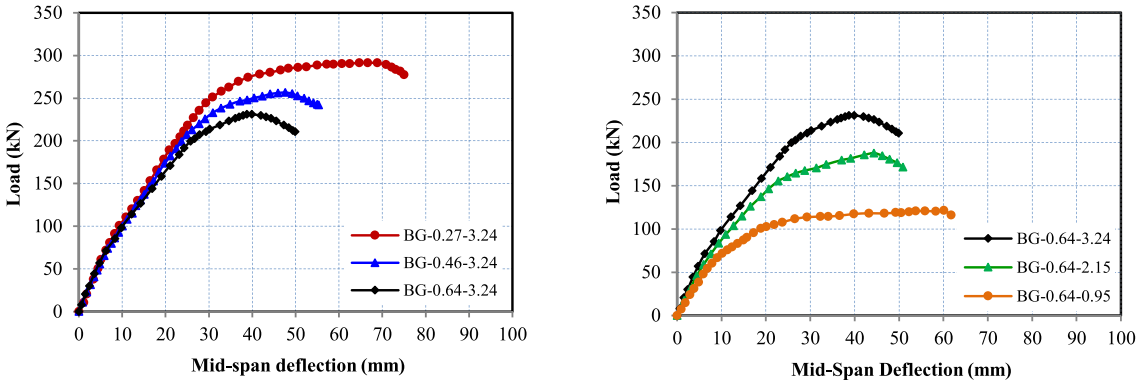


(d) Box girder BG-0.64-2.15



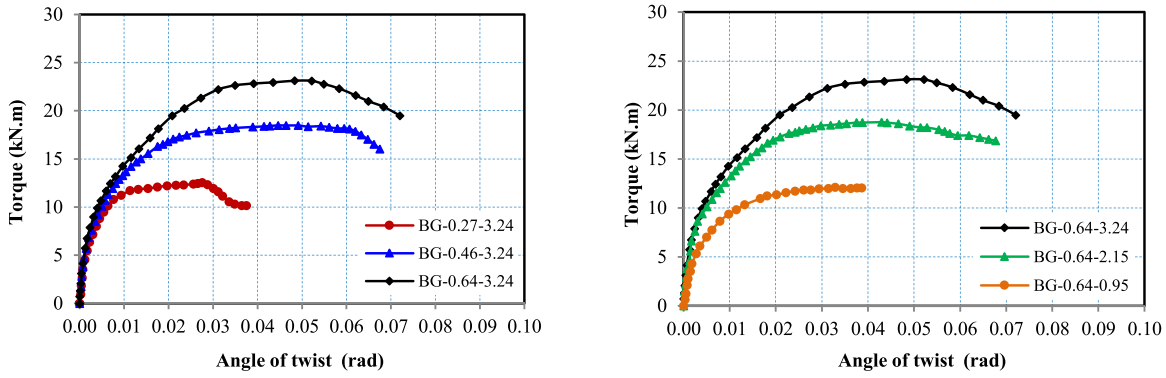
(e) Box girder BG-0.64-0.95

Fig. 3. (*continued*).



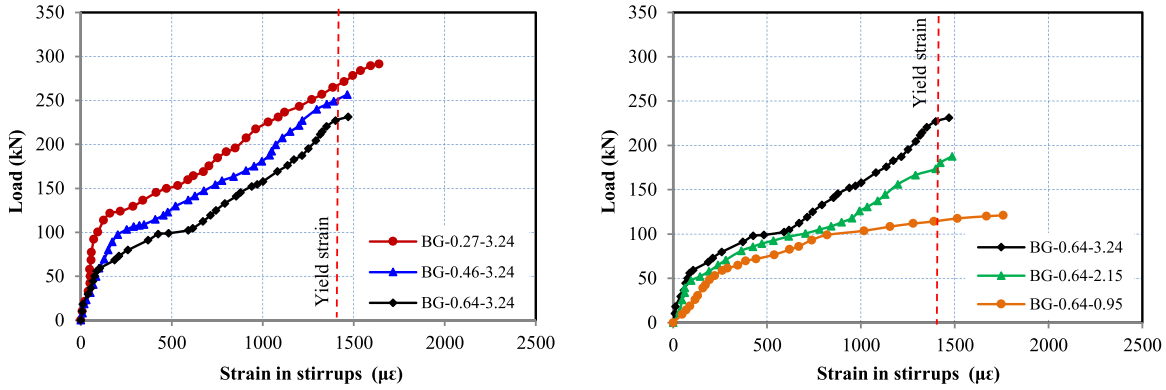
(a) Effect of torsion to shear-depth ratio (b) Effect of longitudinal tensile reinforcement ratio

Fig. 4. Load versus vertical deflection for all tested SCRC box girders.



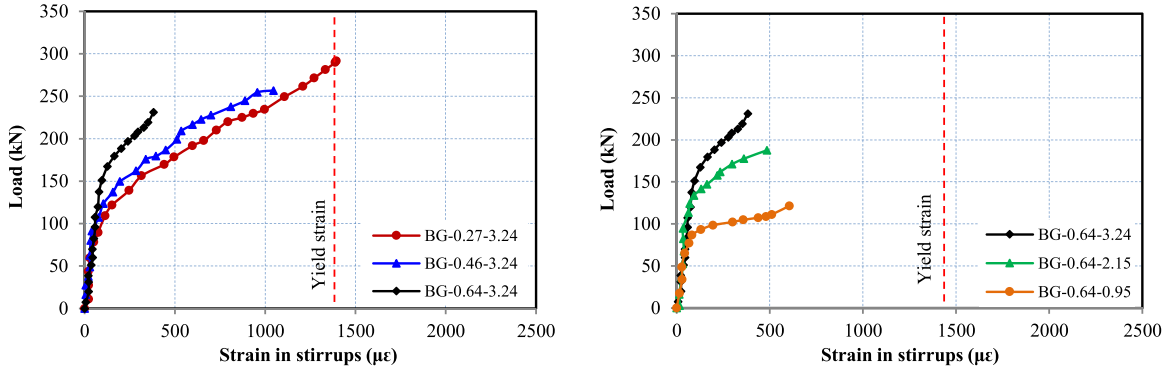
(a) Effect of torsion to shear-depth ratio (b) Effect of longitudinal tensile reinforcement ratio

Fig. 5. Torsion versus angle of twist for all tested SCRC box girders.



(a) Effect of torsion to shear-depth ratio (b) Effect of longitudinal tensile reinforcement ratio

Fig. 6. Load versus strain in transverse reinforcement for all tested SCRC box girders (front face).



(a) Effect of torsion to shear-depth ratio (b) Effect of longitudinal tensile reinforcement ratio

Fig. 7. Load versus strain in transverse reinforcement for all tested SCRC box girders (back face).

twist response, stiffness, strain analysis, and energy absorption.

4.1. Crack patterns, modes of failure, and ultimate capacity

Images of the crack patterns after complete failure for the front (normal view) and back (flipped view) sides of all tested SCRC box girders are shown in Fig. 3a through e. Three specimens were tested at the same longitudinal tensile reinforcement ratio of 3.24 % to investigate the impact of the torsion to shear-depth ratio (T/Vd = 0.27 %, 0.46 %, or 0.64 %) on the performance of SCRC box girders under combined loading. In box girder BG-0.27–3.24, flexural cracks initiated near the mid-span at a load of 45 kN (15.4 % of the ultimate load). Proceeding with loading, the diagonal crack started to emerge in the test zone adjacent to the support at a load of 120 kN (41.2 % of the ultimate load), as shown in Fig. 3a. Subsequently, the width of the first diagonal crack widened until the specimen failed in the test zone due to yielding of transverse reinforcements (shear failure), reaching an ultimate load of 291.4 kN.

As for the tested box girder BG-0.46–3.24, flexural cracks began at a load of 43 kN (16.8 % of the ultimate load), and then additional flexural

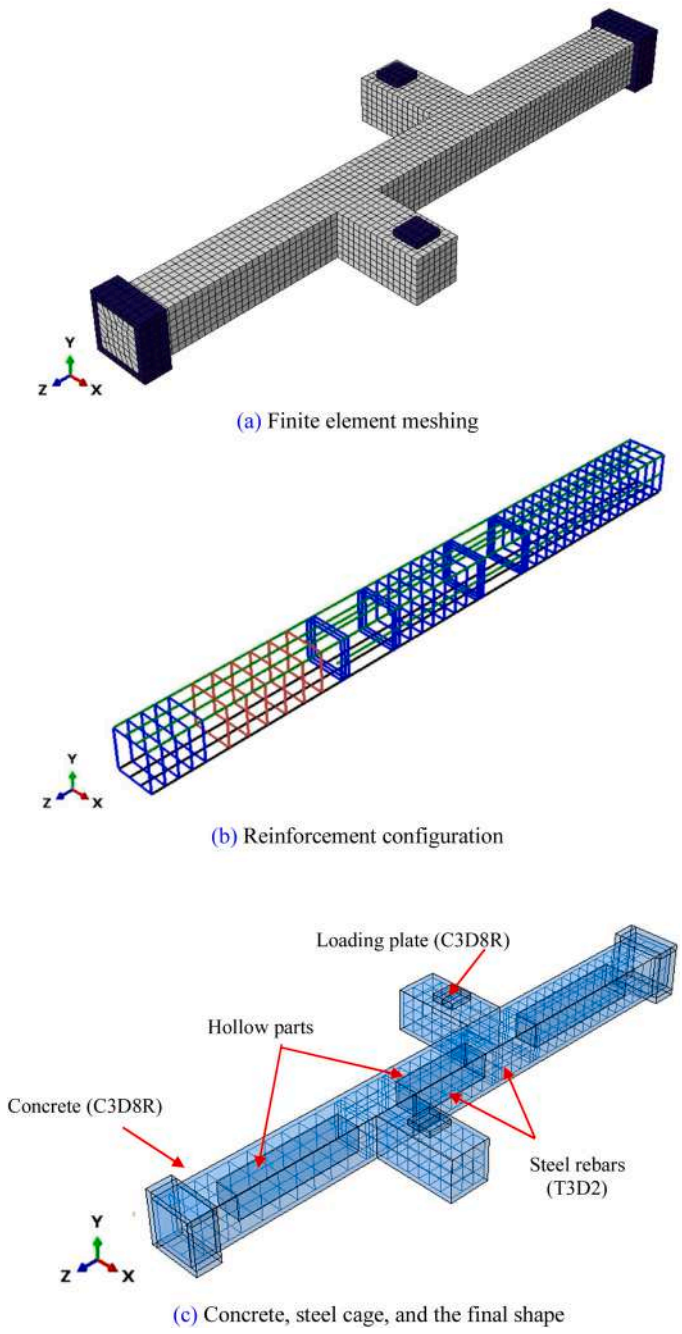


Fig. 8. Finite element simulation of SCRC box girder.

cracks appeared and propagated. At a load of 77 kN (about 30.0 % of the ultimate load), the first shear crack started in the test zone. With further loading, diagonal cracks gradually extended and widened, and the box girder continued to sustain the load up to a load of 256.7 kN until the recorded load declined. Shortly after the failure occurred due to the yielding of transverse reinforcements at the test zone, concrete crushing occurred at mid-span, as depicted in Fig. 3b. Regarding the box girder BG-0.64–3.24, the highest tested T/Vd ratio, flexural cracks appeared at a load of 43 kN (18.6 % of the ultimate load) at mid-span. As the load reached up to 62 kN (26.8 % of the ultimate load), diagonal cracks started to show off (see Fig. 3c). With ongoing loading, flexural and shear cracks spread until the complete shear failure was reached at a load of approximately 231.2 kN. Notably, increasing T/Vd from 0.27 % (specimen BG-0.27–3.24) to 0.64 % (specimen BG-0.64–3.24) not only accelerated the appearance of diagonal cracks in the test zone but also decreased the ultimate capacity.

It was observed that increasing T/Vd from 0.27 % to 0.64 % led to a change in the cracking pattern. The number and width of diagonal cracks increased on the front side rather than the back side of the tested box girders, as the shear and torsional stresses are cumulative. The specimens BG-0.27–3.24, BG-0.46–3.24, and BG-0.64–3.24 failed due to the dominating shear force, which manifested as diagonal cracks in the test zone parallel to each other on both sides (front and back). On the contrary, in the middle zone, cracks on the front and back sides were perpendicular to each other, as this zone was subjected only to pure torsion. It is worth mentioning that the bottom longitudinal reinforcements experienced tensile stresses (positive) due to a simultaneous combination of flexure and torsion. Referring to Tables 3 and 4, it is evident that none of these reinforcements have achieved yielding strain up to failure.

Regarding the effect of the bottom longitudinal tensile reinforcement ratio (ρ_l) on the behavior of SCRC box girders under combined loading, specimens were tested using ρ_l of 3.24 %, 2.15 %, and 0.95 % at the same T/Vd ratio of 0.64 %. The first flexural crack for box girders BG-0.64–2.15 and BG-0.64–0.95 appeared at almost the same loads, around 40 kN. For the box girder BG-0.64–2.15 (see Fig. 3d), additional flexural cracks appeared and spread from the mid-span of the box girder toward the supports until the first diagonal crack manifested at a load of about 63 kN (33.6 % of the ultimate load). Then, the box girder continued to sustain loading until a load of 187.6 kN; at this instant, the reported load began to fall. As well, box girder BG-0.64–0.95 (see Fig. 3e) exhibited a more pronounced decline in behavior compared to box girder BG-0.64–2.15 from the cracking load and the ultimate capacity perspectives, which recorded 55 kN (45.3 % of the ultimate load) and 121.5 kN, respectively. Logically, the decrease in longitudinal tensile reinforcement ratio accelerates the flexural cracking, which in turn leads to early degradation and larger associated ultimate bottom steel strain values without reaching a considerable capacity; see Table 4.

4.2. Load-deflection response

The applied load versus the net vertical mid-span deflection relationships at different loading stages for all tested SCRC box girders are illustrated in Fig. 4. It is evident that all box girders exhibited linear behavior until the point of crack initiation, after which their stiffness began to decrease. As the ultimate load approached, nonlinear behavior became more obvious due to the formation of some plastic deformations and excessive cracking. The values of the net mid-span deflections corresponding to the cracking ($\triangle_{cr}$), yield ($\triangle_y$), ultimate loads ($\triangle_u$), flexural stiffness (K_f), and torsional stiffness (K_T) are listed in Table 4. It is worth noting that the yielding deflection was theoretically computed according to the general yielding approach suggested in Baraghith et al. [76] and Atta et al. [77].

Table 5
Analysis of mesh convergence for specimen BG-0.64–3.24.

Mesh ID	Mesh Size (mm)	Ultimate load (kN)				Ultimate mid-span deflection (mm)			
		$P_{u,\ EXP}$	$P_{u,\ FE}$	$P_{u,FE}/P_{u,Exp}$	% Difference	$\Delta_{u,EXP}$	$\Delta_{u,\ FE}$	$\Delta_{u,FE}/\Delta_{u,EXP}$	% Difference
M20	20	231.2	238.1	1.03	3	38.72	43.3	1.12	12
M30	30	231.2	227.4	0.98	2	38.72	40.01	1.03	3
M40	40	231.2	219.1	0.95	5	38.72	41.08	1.06	6

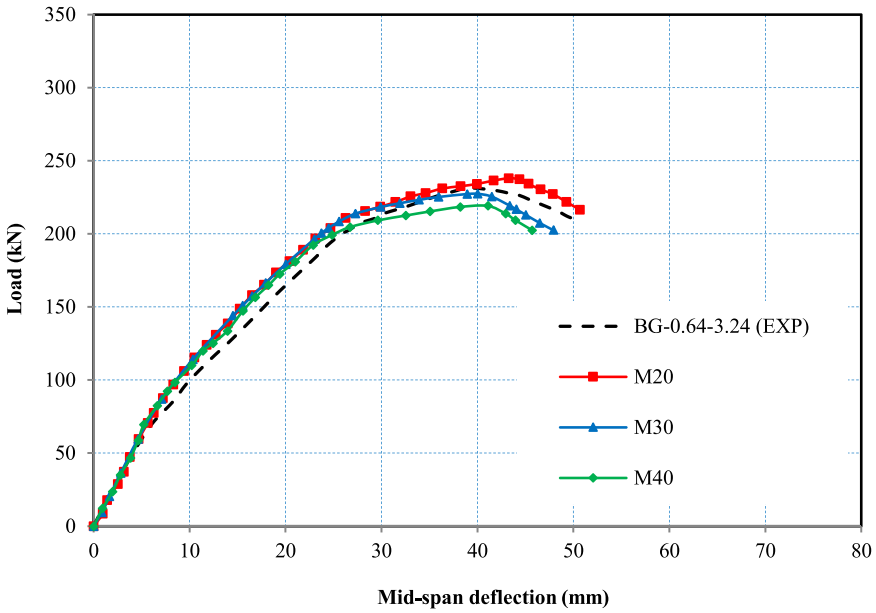
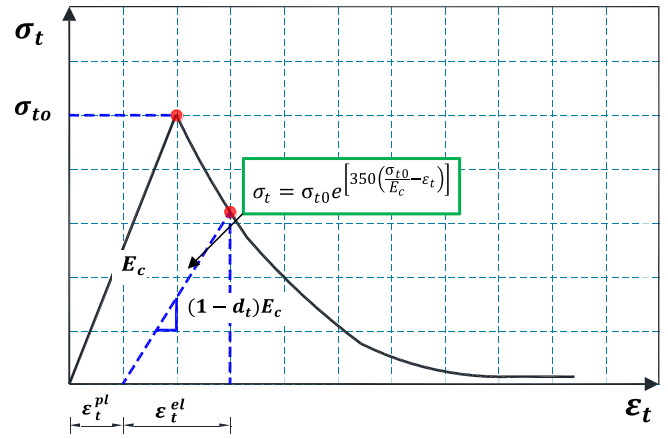
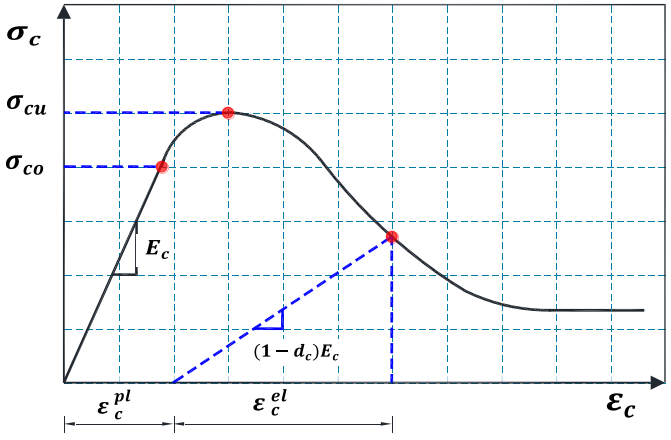


Fig. 9. Load-deflection relationships of mesh convergence for specimen BG-0.64–3.24.



(a) Uniaxial tensile stress-strain response for concrete



(b) Uniaxial compressive stress-strain response for concrete

Fig. 10. Uniaxial stress-strain responses for concrete.

Considering different torsion to shear-depth ratios (T/Vd = 0.27 %, 0.46 %, and 0.64 %), it can be perceived that specimens with a higher T/Vd ratio recorded much larger deflection values compared to their counterparts at the same loading level due to the increasing excessive diagonal cracks (see Fig. 4a). On the other hand, the box girder BG-0.64–0.95, with the lowest bottom longitudinal reinforcement ratio (ρ_l), undergoes a much larger deflection than box girders BG-0.64–2.15 and BG-0.64–3.24, as depicted in Fig. 4b. It may be attributed to the fact that the lower longitudinal reinforcement ratio yields to rapid cracking and then higher deflection. Furthermore, decreasing the ρ_l ratio from 3.24 % to 0.95 % resulted in severe degradation of the cracked flexural stiffness by about 76 %. For the reader's information, the SCRC box girder's uncracked flexural stiffness was calculated as the slope of the load-deflection curve [78,79], whereas the cracked flexural stiffness was determined through the equation $K_{fcr} = (P_u - P_{cr})/(\triangle_u - \triangle_{cr})$ [55], where P_{cr} and P_u are the cracking and ultimate loads, respectively.

4.3. Torque-angle of twist response

According to Fig. 5, the relationships between the measured angle of twist and the applied torque are almost linear up to the first crack, indicating that the members are in the elastic region. The uncracked torsional stiffness can be determined using the equation $K_{Tun} = T_{cr}/\varphi_{cr}$ and listed in Table 4, where T_{cr} is the cracking torque and φ_{cr} is the corresponding cracking twist angle. After cracking, torsional stiffness drops noticeably ($K_{Tcr} = (T_u - T_{cr})/(\varphi_u - \varphi_{cr})$) [1]; at this point, the elements fall within an elastic-plastic stage, where T_u denotes the ultimate torque and φ_u represents the corresponding ultimate twist angle. It can be seen that specimen BG-0.64–3.24, with the highest T/Vd ratio, had greater torsional capacity (23.1 kN.m), ultimate angle of twist (0.0484 rad), and torsional stiffness (both uncracked and cracked) than that for specimen BG-0.46–3.24, which was in turn higher than that for specimen BG-0.27–3.24. As for the effect of the longitudinal tensile reinforcement ratio, the box girder BG-0.64–3.24 ($\rho_l = 3.24\%$) outperformed their counterparts in terms of torsional stiffness and occupied the top of the rank with the maximum ultimate torsional capacity and angle of twist, followed by box girders BG-0.64–2.15 and BG-0.64–0.95.

The investigation into the flexural and torsional stiffness values presented in Table 4 reveals that torsional stiffness generally decreases at the cracking torque at a significantly higher rate than flexural stiffness does at the cracking moment. For example, in specimen BG-0.64–3.24, torsional stiffness experienced a reduction of approximately 90.1 % at the cracking torque, whereas the flexural stiffness decreased by about 49.7 % at the cracking moment. Furthermore, as the tensile longitudinal

Table 6
The required CDPM parameters.

Dilation angle	Eccentricity	Stress ratio (f_{bo}/f_{co})	Shape factor (K)	Viscosity parameter	ν	ε_o	ε_{cu}
32°	0.1	1.16	0.667	0	0.22	0.2 %	0.35 %

f_{bo}/f_{co}= the ratio between the biaxial to uniaxial stresses; ν = Poisson's ratio; ε_o = the concrete crushing strain; ε_{cu} = the concrete strain corresponding to maximum compressive cylinder strength.

reinforcement ratio decreased, the disparity between these degradation rates became less pronounced. In the case of specimen BG-0.64–0.95, for instance, torsional stiffness declined by about 88.6 % at the cracking torque, while the flexural stiffness dropped by around 84.5 % at the cracking moment.

4.4. Developed normal strain on stirrups

The developed strains were measured at the middle vertical stirrup in the test zone (both front and back sides); see Fig. 1. The relationships of the load-strain in stirrups are illustrated in Figs. 6 and 7, with the dashed line representing the yield strain value of the transverse reinforcement (about 1400 με), as shown in Table 3. Prior to the onset of shear cracking, the recorded strain levels were negligible. During the post-cracking stage, the strain in the steel stirrups began to increase, indicating their effective contribution in resisting the developed stresses.

It is worth mentioning that the stress on the front side of the stirrup resulted from the sum of shear and torsion (additive side). Vice versa, the shear and torsional stresses are subtractive on the stirrup back side. The maximum stirrup strain values recorded in the front side were 1640, 1465, 1470, 1486, and 1759 με for tested box girders BG-0.27–3.24, BG-0.46–3.24, BG-0.64–3.24, BG-0.64–2.15, and BG-0.64–0.95, respectively. This illustrates that all tested box girders failed in the test zone, and the strains in the vertical stirrups (front side) exceeded the yielding stress; see Fig. 6. On the other hand, the maximum stirrup strain values recorded in the back side for the box girders BG-0.27–3.24, BG-0.46–3.24, BG-0.64–3.24, BG-0.64–2.15, and BG-0.64–0.95 were 1395, 1046, 381, 502, and 605 με, respectively. Accordingly, the vertical stirrups (back side) in all tested box girders haven't reached their yield strains up to failure; see Fig. 7.

4.5. Energy absorption (E)

To determine the energy absorption, the area under the load-deflection curve was integrated up to failure [80]. The values of the energy absorption for all tested SCRC box girders are reported in Table 4. With regard to the torsion to shear-depth ratios (0.27 %, 0.46 %, and 0.64 %), as expected, the energy absorption values were inversely proportional to the T/Vd ratio. The energy absorption for specimen BG-0.27–3.24 was 15019 kN·mm, which is more than twice the value of specimen BG-0.64–3.24 (6370 kN·mm), keeping the same ρ_l. It may be attributed to the fact that when the torsional moment increases, excessive diagonal cracks spread and widen, which in turn causes the brittle shear failure. Considering the specimens with variable longitudinal tensile reinforcement ratios (3.24 %, 2.15 %, and 0.95 %), a slight increase was observed with decreasing ρ_l, which may be attributed to the tensile-controlled failure that is obtained in such cases. For example, the values of energy absorption were 6370, 6809, and 6921 kN·mm for specimens BG-0.64–3.24, BG-0.64–2.15, and BG-0.64–0.95, respectively.

5. Finite element analysis (FEA)

Due to the high cost and scarcity of experimental data, advanced software plays an essential role in civil engineering applications. Nonlinear three-dimensional finite element modeling (FEM) is used in this work to simulate the behavior of tested SCRC box girders under combined bending, shear, and torsion loads using ABAQUS software [58]. The simulation was thoroughly validated by comparing with experimental results to guarantee accuracy and reliability. Next, a parametric study was performed to investigate the impact of different parameters. Different ratios of torsion to shear-depth (T/Vd) and longitudinal reinforcement (ρ_l), as well as the transverse reinforcement ratio (ρ_t) and the wall thickness to width ratio (t_w/b) have been studied.

5.1. Model built-up

Fig. 8 depicts the finite element mesh used in the current study. An eight-node quadratic tetrahedron C3D8R solid element was used to model the concrete section and the steel plates. This element activates the three translational degrees of freedom at each node. Additionally, the longitudinal reinforcement and the shear stirrups were simulated using a two-node linear 3D truss element T3D2 to transfer only axial stresses.

An incremental mechanism was proposed to apply the vertical load on the center of the steel plates. Supports were defined as rigid bodies constrained against movement and rotation in the lateral directions. Additionally, the support surfaces were characterized as rough, allowing friction force to resist the beam's elongation and contraction due to the formation of cracks.

After simulating the geometry of the tested box girder, a sensitivity analysis was performed on specimen BG-0.64–3.24 to calibrate the model based on alternative mesh sizes (20 mm, 30 mm, or 40 mm); see Table 5. It is evident that the mesh size of 30 mm offers the closest result to the experimental counterpart in terms of both ultimate load and the corresponding mid-span deflection as depicted in Fig. 9, while also ensuring reasonable job time. Therefore, this mesh size was utilized in both the FEM validation and the parametric study.

5.2. Material modeling

The concrete damage plasticity model (CDP) was utilized to define the elastic and plastic characteristics of concrete. This model takes into consideration the degradation of concrete and assumes compressive crushing and tensile cracking as the two main failure mechanisms of concrete. In other words, the CDP model considers tension stiffening and compressive softening together with tension and compression damage of concrete. To specify the post-peak tension failure behavior of concrete, the fracture energy method was used, while the fracture energy (G_f) can be estimated by the equation proposed by Hillerborg [81], as shown in Fig. 10a. Based on the formulae stipulated in the ACI 318–25 Code [49], the uniaxial compressive stress-strain curve for concrete was constructed considering the relationship suggested by Park and Paulay [82]; see Fig. 10b. The modeling parameters for concrete as used in ABAQUS [58], such as the ratio between the dilation angle ($\varnothing$), the biaxial and uniaxial stresses (f_{bo}/f_{co}), the shape factor for yield surface (K), the viscosity parameter, Poisson's ratio (ν), the concrete strain corresponding to maximum compressive cylinder strength (ε_o), and the concrete crushing strain (ε_{cu}) are summarized in Table 6.

The response of steel material may be represented by a bilinear elastic-plastic stress-strain relationship with strain hardening in both tension and compression. The key input data for the mechanical properties of steel (yield and ultimate stress) were inserted as experimentally

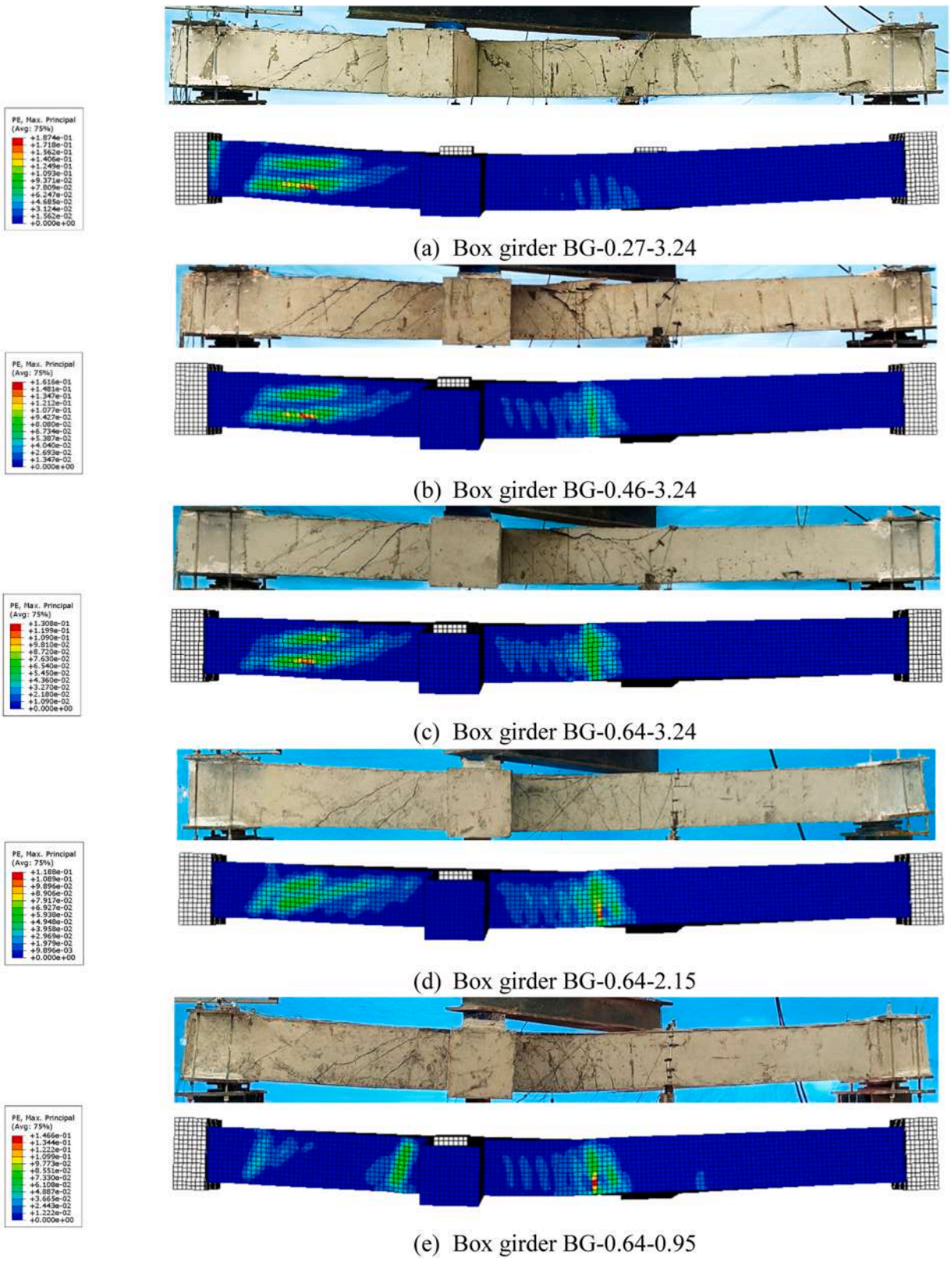
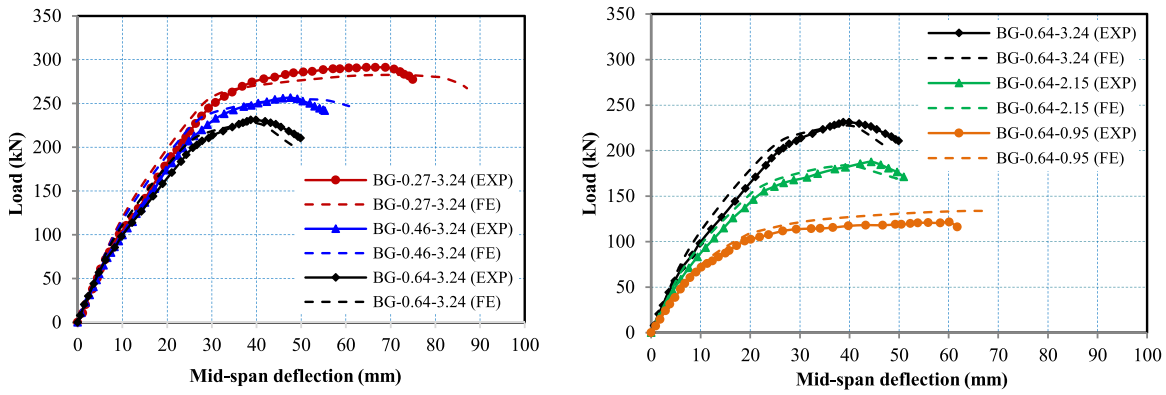


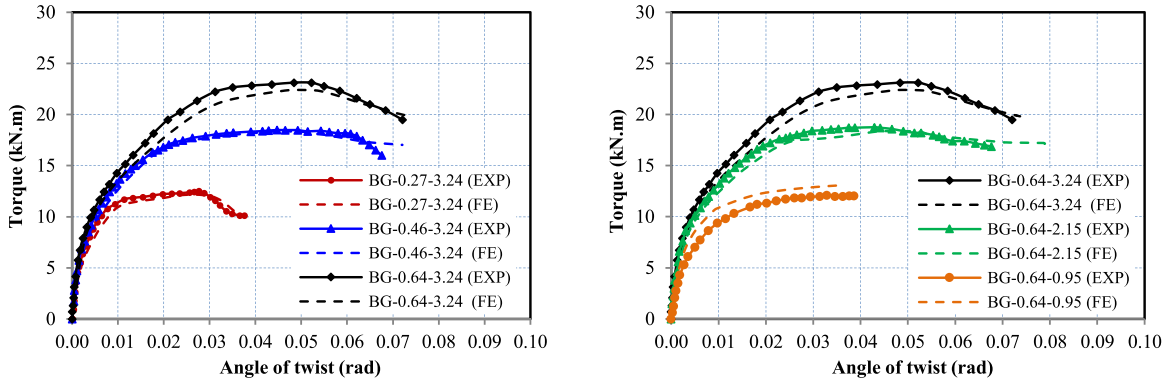
Fig. 11. Experimental versus numerical failure patterns for all tested SCRC box girders.

specified in Table 3. Since the steel reinforcement did not slip from the tested SCRC box girders, it was modeled as completely bonded through the embedded region method, likely due to the use of indentations and sufficient development lengths. In addition, 25 mm thick steel plates were positioned underneath the loading points as well as at the supporting points and were simulated as a linear elastic material. It should be noted that the aforementioned plates were used to uniformly distribute the applied loads and avoid local concrete failure. The elastic modulus of the steel was 200 GPa, and Poisson's ratio was 0.3.



(a) Effect of torsion to shear-depth ratio (b) Effect of longitudinal tensile reinforcement ratio

Fig. 12. Experimental versus numerical load-deflection relationships for all tested SCRC box girders.



(a) Effect of torsion to shear-depth ratio (b) Effect of longitudinal tensile reinforcement ratio

Fig. 13. Experimental versus numerical torque-angle of twist relationships for all tested SCRC box girders.

Table 7
Model verification.

Specimen ID	Ultimate load (kN)			Ultimate mid-span deflection (mm)			Ultimate torque (kN.m)			Ultimate angle of twist (rad)		
	$P_{u,\ EXP}$	$P_{u,\ FE}$	$P_{u,FE}/P_{u,Exp}$	$\Delta_{u,EXP}$	$\Delta_{u,\ FE}$	$\Delta_{u,FE}/\Delta_{u,EXP}$	$T_{u,\ EXP}$	$T_{u,\ FE}$	$T_{u,\ FE}/T_{u,EXP}$	$\Phi_{u,\ EXP}$	$\Phi_{u,\ FE}$	$\Phi_{u,FE}/\Phi_{u,EXP}$
BG-0.27–3.24	291.4	282.8	0.97	64.64	70.29	1.09	12.5	12.2	0.98	0.0276	0.0266	0.96
BG-0.46–3.24	256.7	254.9	0.99	47.61	50.54	1.06	18.5	18.3	0.99	0.0447	0.0458	1.02
BG-0.64–3.24	231.2	227.4	0.98	38.72	40.01	1.03	23.1	22.4	0.97	0.0484	0.0481	0.99
BG-0.64–2.15	187.6	183.8	0.98	44.36	39.31	0.89	18.8	18.4	0.98	0.0429	0.0472	1.10
BG-0.64–0.95	121.5	133.7	1.10	60.09	63.51	1.06	12.2	13.1	1.07	0.0329	0.0351	1.07
Average			1.004			1.026			0.998			1.028
Standard deviation			0.048			0.071			0.037			0.051
Coefficient of variation			4.78 %			6.92 %			3.71 %			4.96 %

5.3. *Verification of the numerical model against the experimental results*

All tested SCRC box girders in the experimental program were modeled using finite element analysis (ABAQUS software [58]). Comparisons between the experimental results and numerical analysis were made to examine the efficiency of the adopted FEM. The verification will be discussed in terms of failure mode (Fig. 11), ultimate loads, load-deflection behavior (Fig. 12), and torque-twist response (Fig. 13). It was obvious that the distinct failure modes for all tested SCRC box girders are accurately simulated, demonstrating good agreement. A detailed comparison between the experimental and numerical ultimate loads and the associated mid-span deflections, as well as ultimate torques and the associated angles of twist is provided in Table 7. The average ratio and the coefficient of variation between the numerical ultimate load ($P_{u,\ FE}$) and the experimental ones ($P_{u,\ EXP}$) are 1.004 and 4.78 %, respectively. Additionally, there is an insignificant discrepancy between the numerical ultimate mid-span deflection ($\Delta_{max,\ FE}$) and that obtained experimentally ($\Delta_{max,\ EXP}$) with an average ratio and coefficient of variation of 1.026 and 6.92 %, respectively. In the same vein, when the ultimate torque is taken into account, these ratios are 0.998 and 3.71 %, respectively. As well, these specific ratios of the ultimate corresponding angle of twist are 1.028 and 4.96 %, respectively. All in all, the FEM accurately predicted the overall experimental performance of all tested SCRC box girders.

Table 8
Modeled SCRC box girders.

Group No.	Specimen ID	e (mm)	T/Vd	ρ_l%	ρ_t%	t_w/b	Objectives
1	BG-0.18–3.24–0.25–0.21	200	0.18	3.24	0.25	0.21	Studying the effect of torsion to shear-depth ratio (T/Vd)
	BG-0.37–3.24–0.25–0.21	400	0.37				
	BG-0.55–3.24–0.25–0.21	600	0.55				
	BG-0.73–3.24–0.25–0.21	800	0.73				
	BG-0.92–3.24–0.25–0.21	1000	0.92				
2	BG-0.64–1.29–0.25–0.21	700	0.64	1.29			Studying the effect of bottom longitudinal tensile reinforcement ratio (ρ_l)
	BG-0.64–1.70–0.25–0.21			1.70			
	BG-0.64–2.67–0.25–0.21			2.67			
	BG-0.64–3.55–0.25–0.21			3.55			
	BG-0.64–4.20–0.25–0.21			4.20			
3	BG-0.64–3.24–0.19–0.21			3.24	0.19		Studying the effect of transverse reinforcement ratio (ρ_t)
	BG-0.64–3.24–0.37–0.21				0.37		
	BG-0.64–3.24–0.67–0.21				0.67		
	BG-0.64–3.24–1.05–0.21				1.05		
	BG-0.64–3.24–1.50–0.21				1.50		
4	BG-0.64–3.24–0.25–0.17				0.25	0.17	Studying the effect of wall thickness to width ratio (t_w/b)
	BG-0.64–3.24–0.25–0.26					0.26	
	BG-0.64–3.24–0.25–0.30					0.30	
	BG-0.64–3.24–0.25–0.34					0.34	

Where e = the load eccentricity from the center of the box girder; T/Vd = the torsion to shear-depth ratio; ρ_l = the bottom longitudinal tensile reinforcement ratio; ρ_t = the transverse reinforcement ratio at the test zone; t_w/b = the wall thickness to width ratio.

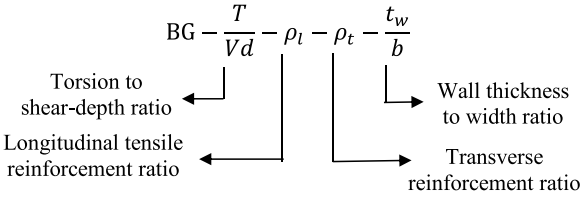


Fig. 14. Specimen's designation for all modeled SCRC box girders.

6. Parametric study

This section discusses the effects of different parameters on the behavior of SCRC box girders subjected to combined loading (bending, shear, and torsion), as detailed in Table 8. The designation of the analyzed SCRC box girders is a five-part name (see Fig. 14), where the first part denotes a box girder. The second part represents the torsion to shear-depth ratio (T/Vd), the third part identifies the bottom longitudinal tensile reinforcement ratio (ρ_l), the fourth part specifies the transverse reinforcement ratio (ρ_t), and finally the fifth part indicates the wall thickness to width ratio (t_w/b). The predicted numerical ultimate load, the corresponding deflection, the ultimate torque, the associated angle of twist, the ultimate strain in both longitudinal and transverse reinforcements (front and back sides), and energy absorption for all modeled SCRC box girders are shown in Table 9.

6.1. *Effect of the torsion to shear-depth ratio* (T/Vd)

Five SCRC box girders with identical dimensions and reinforcements (group No. 1) were numerically analyzed at various torsion to shear-depth ratios ranging from 0.18 % to 0.92 %, as detailed in Table 8. Specimens exhibiting a T/Vd ratio < 0.55 %, specifically BG-0.18–3.24–0.25–0.21 and BG-0.37–3.24–0.25–0.21, failed due to the

Table 9
Numerical results for all analyzed SCRC box girders.

Group No.	Specimen ID	P_u (kN)	$\triangle_u$ (mm)	T_u (kN.m)	φ_u (rad)	S_l (με)	S_{tf} (με)	S_{tb} (με)	E (kN.mm)
1	BG-0.18–3.24–0.25–0.21	294.1	74.07	8.5	0.0149	1764	1849	1452	17725
	BG-0.37–3.24–0.25–0.21	268.4	68.07	15.4	0.0415	1782	1498	1163	14477
	BG-0.55–3.24–0.25–0.21	240.5	44.02	20.7	0.0505	1736	1474	314	7538
	BG-0.73–3.24–0.25–0.21	209.4	32.46	23.9	0.0497	1612	1463	144	4466
	BG-0.92–3.24–0.25–0.21	174.3	24.02	25.0	0.0454	1603	1429	57	2540
2	BG-0.64–1.29–0.25–0.21	152.9	55.91	15.3	0.0498	2381	1282	117	6648
	BG-0.64–1.70–0.25–0.21	166.5	45.64	16.7	0.0359	2243	1242	119	6194
	BG-0.64–2.67–0.25–0.21	209.3	40.91	20.9	0.0499	2038	1437	129	6050
	BG-0.64–3.55–0.25–0.21	239.1	34.52	23.9	0.0501	1916	1490	349	5855
	BG-0.64–4.20–0.25–0.21	244.9	33.40	24.5	0.0506	1504	1499	367	5166
3	BG-0.64–3.24–0.19–0.21	217.2	33.05	21.7	0.0426	1616	1409	175	4712
	BG-0.64–3.24–0.37–0.21	231.4	35.23	23.1	0.0445	1921	1444	119	5377
	BG-0.64–3.24–0.67–0.21	246.1	40.91	24.6	0.0524	2033	1309	118	6863
	BG-0.64–3.24–1.05–0.21	253.0	44.11	25.3	0.0576	2044	1288	66	7545
	BG-0.64–3.24–1.50–0.21	255.8	41.93	25.5	0.0526	2042	764	40	7251
4	BG-0.64–3.24–0.25–0.17	199.5	32.30	19.9	0.0455	1638	1482	403	4215
	BG-0.64–3.24–0.25–0.26	229.7	40.23	22.9	0.0542	1753	1489	56	6554
	BG-0.64–3.24–0.25–0.30	240.9	46.03	24.1	0.0612	1768	1510	79	8184
	BG-0.64–3.24–0.25–0.34	251.4	46.43	25.1	0.0601	1773	1428	23	8539

Where P_u = ultimate load; $\triangle_u$= ultimate deflection; T_u = ultimate torque; φ_u = ultimate angle of twist; S_l = maximum strain in the bottom longitudinal tensile reinforcement; S_{tf} = maximum strain in the transverse reinforcement at the middle of the test zone (front side); S_{tb}= maximum strain in the transverse reinforcement at the middle of the test zone (back side); E = the energy absorption.

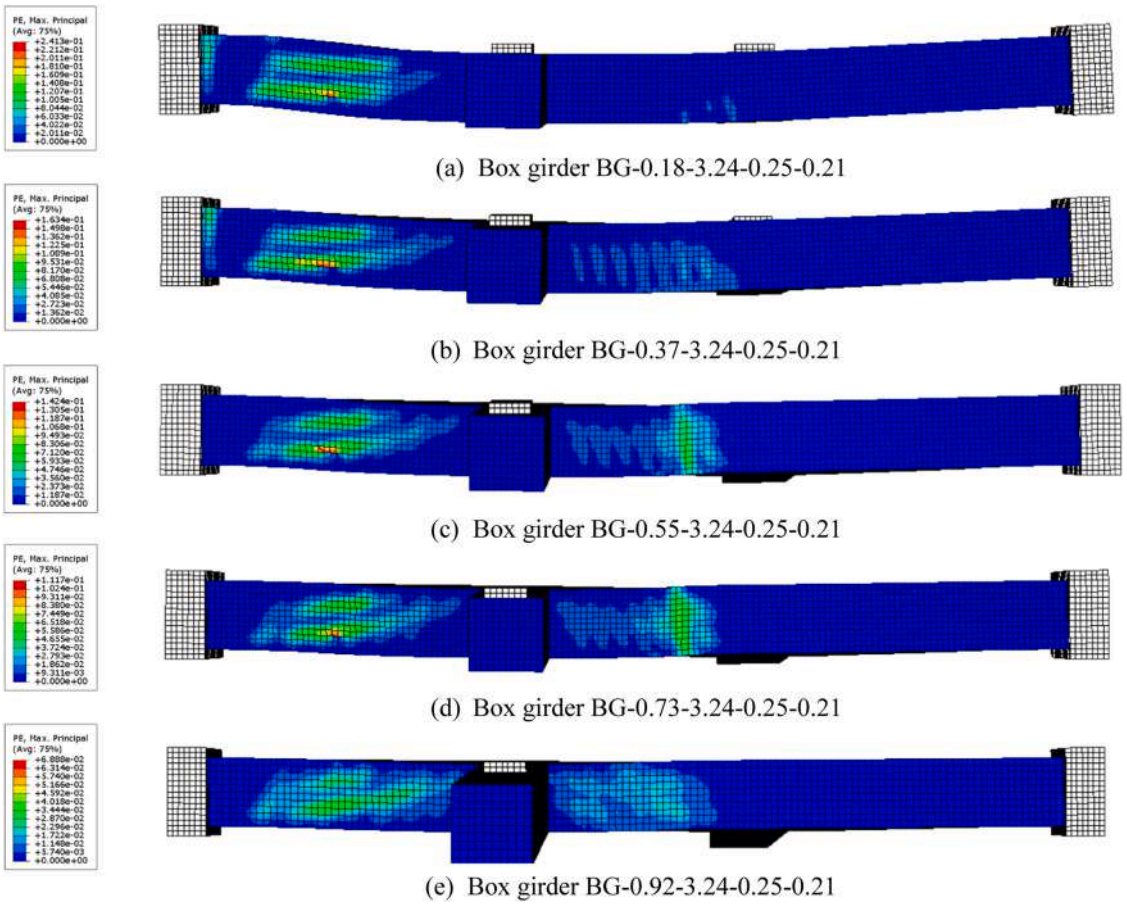


Fig. 15. Effect of torsion to shear-depth ratio (T/Vd) on the failure pattern for the analyzed SCRC box girders.

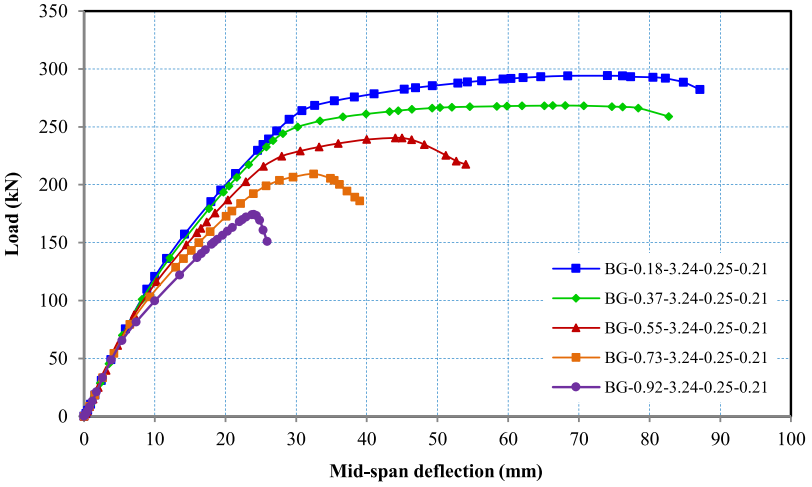


Fig. 16. Effect of torsion to shear-depth ratio (T/Vd) on the load-deflection relationships for the analyzed SCRC box girders.

combined effects of flexural and shear, which were characterized by the major diagonal cracks in the test zone. In contrast, specimens of T/Vd ≥ 0.55 % (BG-0.55–3.24–0.25–0.21, BG-0.73–3.24–0.25–0.21, and BG-0.92–3.24–0.25–0.21) experienced sudden failure due to the development of excessive diagonal cracks (see Fig. 15). This failure was attributed to the combined effects of shear and torsion, with a torsion-dominated accompanied by a drop in ultimate load and a decrease in cross-sectional stiffness. The difference between the ultimate strains on both sides (front and back) of the middle vertical stirrup in the test zone was significant, with yielding occurring only on the front side, confirming the aforementioned mode of failure.

The analyzed SCRC box girders' load-deflection responses at different T/Vd ratios are shown in Fig. 16. The recorded outcomes showed that the ultimate load and the related mid-span deflection of the SCRC box girders significantly reduced when the T/Vd ratio of SCRC box girders increased, which is consistent with the findings of Alnuaimi et al. [54]. The lowest ultimate load and the mid-span deflection were recorded in specimen BG-0.92–3.24–0.25–0.21, which decreased by about 40.7 % and 67.6 %, respectively, compared to its counterpart specimen BG-0.18–3.24–0.25–0.21, as listed in Table 9. Consequently, the

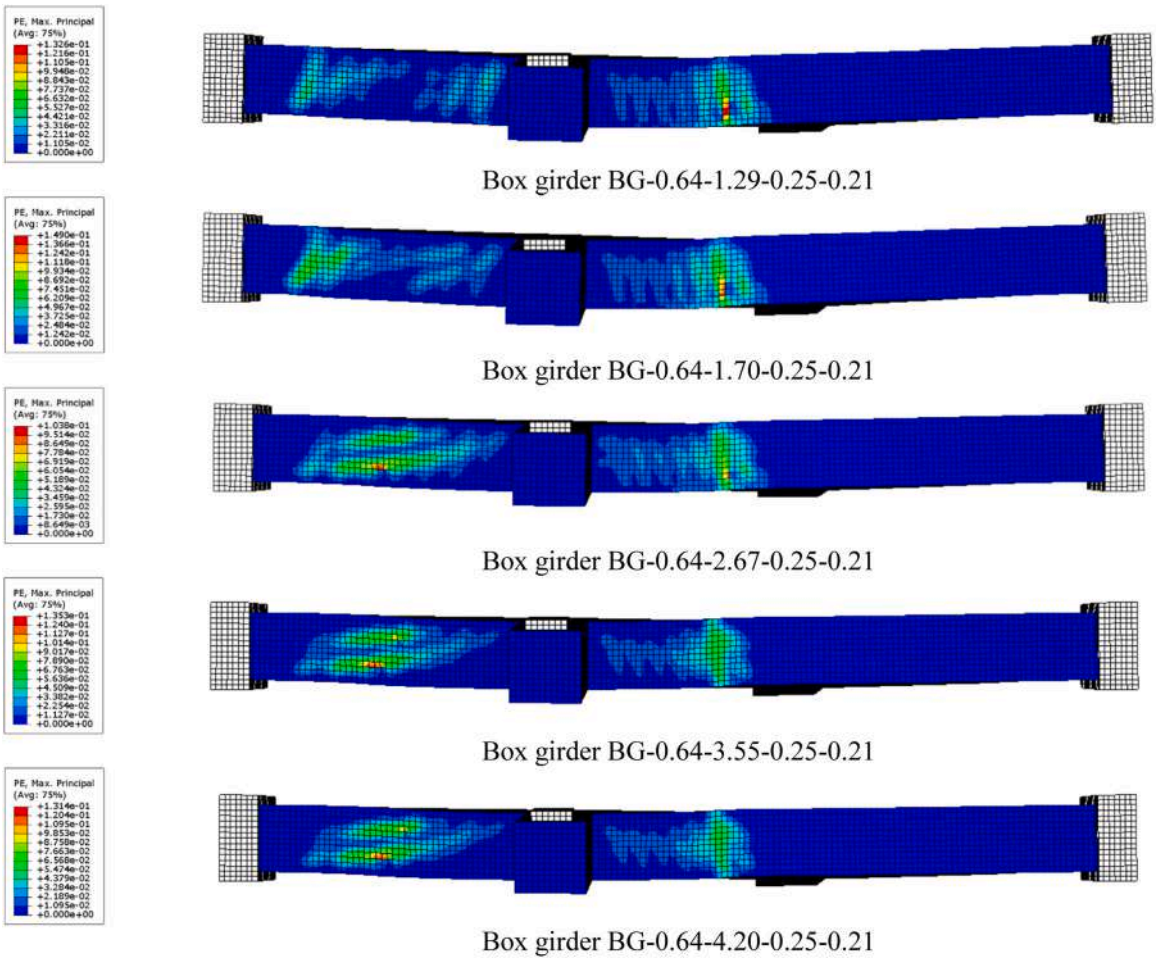


Fig. 17. Effect of the bottom longitudinal tensile reinforcement ratio (ρ_l) on the failure pattern for the analyzed SCRC box girders.

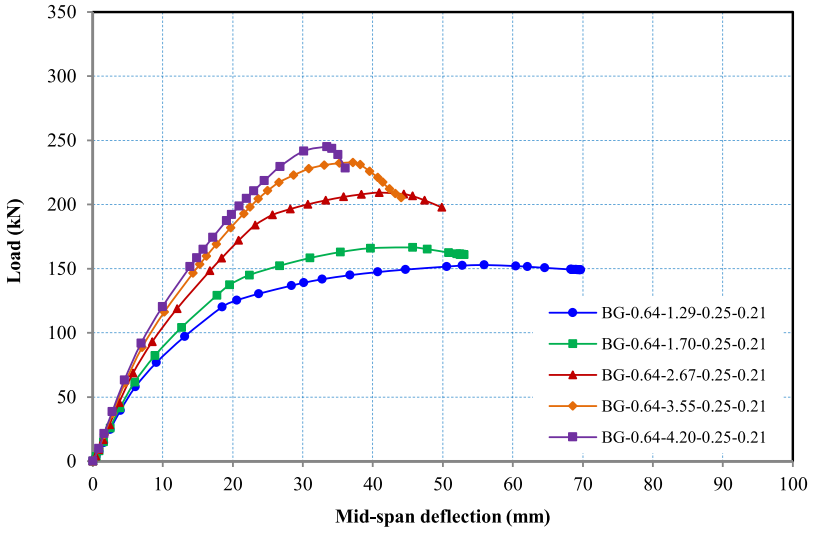


Fig. 18. Effect of bottom longitudinal tensile reinforcement ratio (ρ_l) on the load-deflection relationships for the analyzed SCRC box girders.

analyzed specimens incorporating a higher T/Vd ratio ($\geq$ 0.55 %) yielded lower energy absorption. In sum, the effect of the T/Vd ratio on the behavior of the analyzed SCRC box girders is similar to that found from the experimental study.

6.2. *Effect of the bottom longitudinal tensile reinforcement ratio (ρ_l)*

Group No. 2 consists of five SCRC box girders with varying bottom longitudinal tensile reinforcement ratios (ρ_l = 1.29–4.20 %) as listed in Table 8. Specimens with lower longitudinal tensile reinforcement ratios (ρ_l < 2.67%) failed as a result of flexural cracks that developed in the

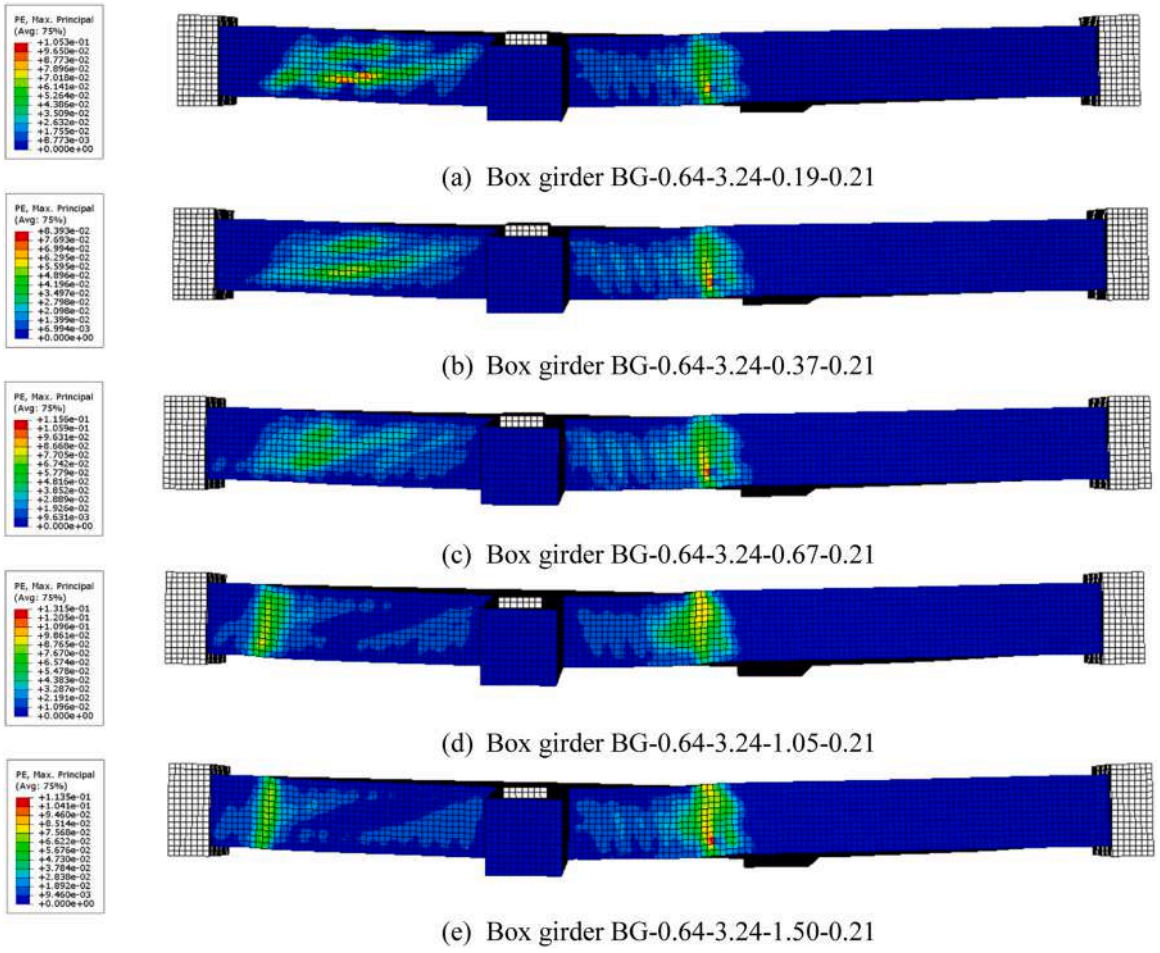


Fig. 19. Effect of transverse reinforcement ratio (ρ_t) on the failure pattern for the analyzed SCRC box girders.

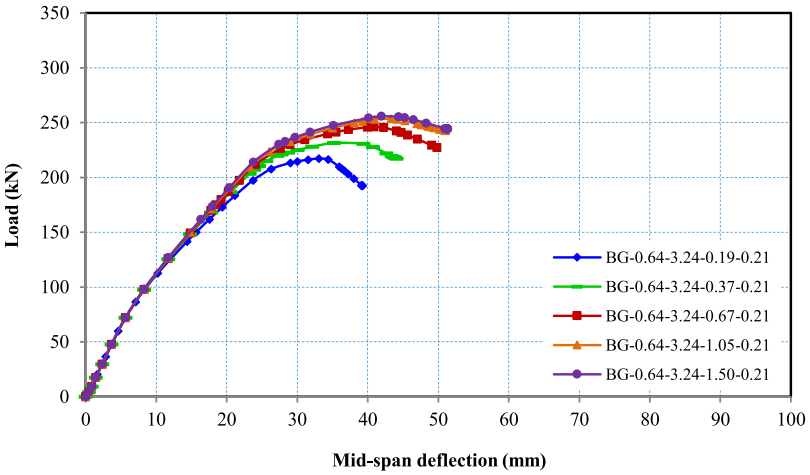


Fig. 20. Effect of transverse reinforcement ratio (ρ_t) on the load-deflection relationships for the analyzed SCRC box girders.

mid-span zone. On the other hand, specimens with ρ_l ratio of 2.67% exhibited yielding of bottom tension steel at the mid-span as well as the front side of the middle vertical stirrup in the test zone simultaneously. As the tension reinforcement ratio increased ($\rho_l > 2.67\%$), diagonal shear cracks became concentrated in the test zone, propagating and widening until shear failure occurred, characterized by torsional domination, as shown in Fig. 17.

As illustrated in Fig. 18, the applied load of specimens with higher longitudinal tensile reinforcement ratios (ρ_l>2.67%) suddenly dropped without a strain-hardening mechanism, unlike counterparts with lower ratios. Generally, increasing the longitudinal tensile reinforcement ratio remarkably improved the capacity of the SCRC box girders. For clarification, the ultimate load of specimen BG-0.64–4.20–0.25–0.21, with the highest ρ_l, showed 1.6 times that for specimen BG-0.64–1.29–0.25–0.21, with the lowest ρ_l. However, this enhancement comes with the loss of the developed ductility, where the exhibited energy absorption of

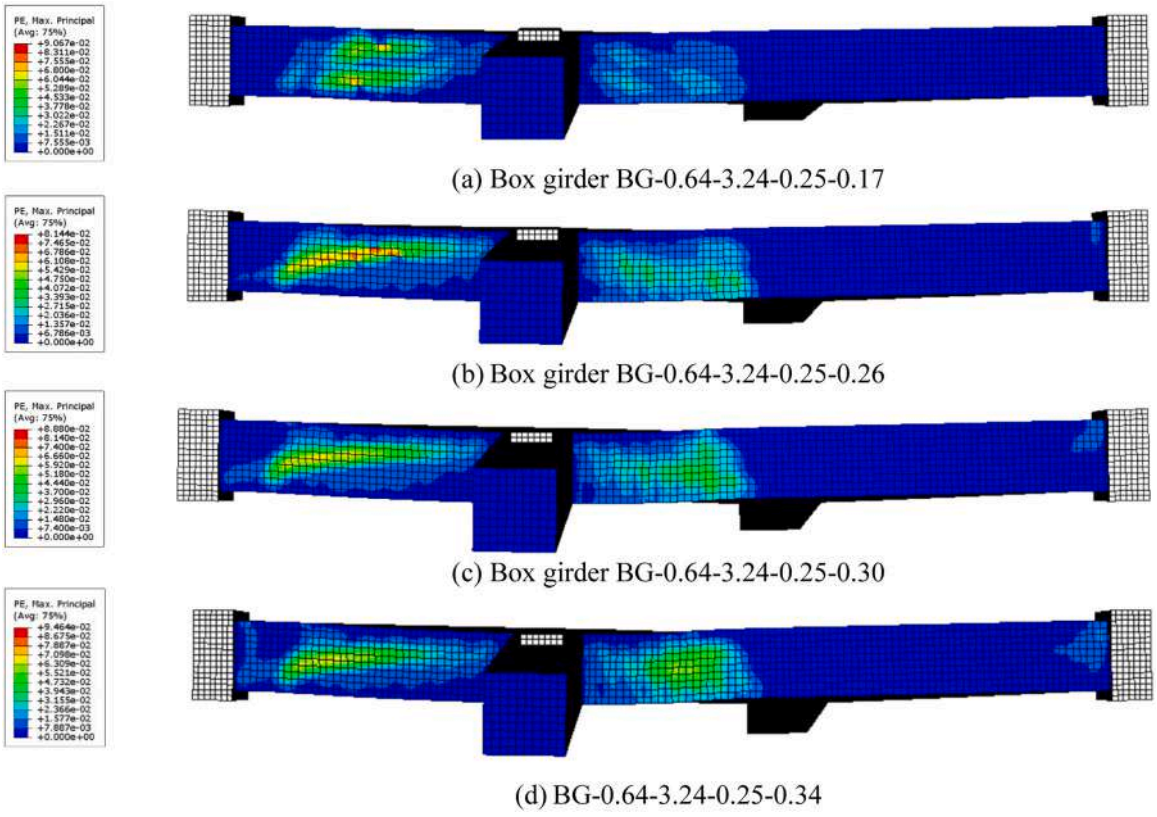


Fig. 21. Effect of wall thickness to width ratio (t_w/b) on the failure pattern for the analyzed SCRC box girders.

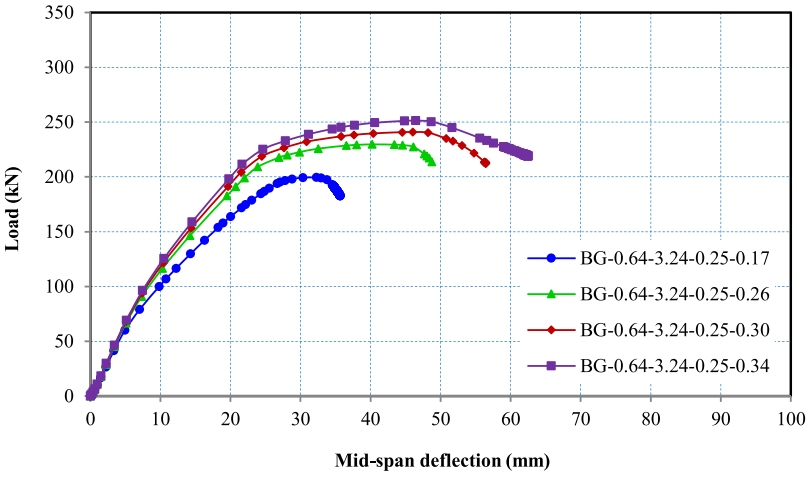


Fig. 22. Effect of wall thickness to width ratio (t_w/b) on the load-deflection relationships for the analyzed SCRC box girders.

specimen BG-0.64–4.20–0.25–0.21 is about 0.78 that developed for specimen BG-0.64–1.29–0.25–0.21 (see Table 9). It is worth mentioning that the higher energy absorption index for SCRC box girders with the lowest ρ_l could be attributed to the flexural-controlled failure.

6.3. *Effect of the transverse reinforcement ratio (ρ_t)*

To examine the effect of the transverse reinforcement ratio (group No. 3), five SCRC box girders with different transverse reinforcement ratios of 0.19 %, 0.37 %, 0.67 %, 1.05 %, and 1.50 % were numerically analyzed at a T/Vd ratio of 0.64 % and ρ_l = 3.24% as detailed in Table 8. The tensile damage variation of the SCRC box girders with variable ρ_t under combined loading is illustrated in Fig. 19. In this group, specimens with $\rho_t < 0.67\%$ exhibited signs of shear failure caused by the spread of diagonal cracks in the test zone with the dominance of torsion. This was confirmed by the differences in stirrup strain observed on both the front and back sides. On the contrary, other specimens with $\rho_t \geq 0.67\%$ demonstrated a flexural failure mode, where the strain of the longitudinal tensile reinforcement reached yielding, unlike transverse reinforcement, as shown in Table 9.

It can be observed that the specimens demonstrated higher capacities as the transverse reinforcement ratio increased. However, when this ratio exceeded 1.05 %, there was a negligible impact on the ultimate load, as the concrete crushed before the steel yielded, as illustrated in Fig. 20. Furthermore, an increase in the transverse reinforcement ratio notably enhanced energy absorption, achieving 7545 kN.mm for the

SCRC box girder BG-0.64–3.24–1.05–0.21, approximately 1.6 times greater than that of BG-0.64–3.24–0.19–0.21.

6.4. Effect of the wall thickness to width ratio (t_w/b)

Four SCRC box girders with different wall thickness to width ratios of 0.17 %, 0.26 %, 0.3 %, and 0.34 % (group No. 4) were numerically analyzed at a T/Vd ratio of 0.64 % as listed in Table 8. All specimens demonstrated shear failure characterized by the development of diagonal cracks in the test zone, associated with flexural cracks in the middle zone, as seen in Fig. 21. In this instance, strain values in the front side of the test zone's mid-stirrup reached yield, unlike the bottom steel, as given in Table 9. The load versus mid-span deflection responses for the analyzed specimens in this group are presented in Fig. 22. It can be seen that increasing the wall thickness to width ratio resulted in the following: 1) The failure load increased for specimen BG-0.64–3.24–0.25–0.34 ($t_w/b = 0.34$ %) by 26.0 % compared to specimen BG-0.64–3.24–0.25–0.17 ($t_w/b = 0.17$ %); 2) there was no noticeable impact on the reinforcements' ultimate strain; and 3) the energy absorption was significantly enhanced at higher wall thickness to width ratios.

7. Conclusion

This paper discusses the results of an experimental and numerical investigation of the behavior of self-compacted reinforced concrete (SCRC) box girders subjected to combined loading (bending, shear, and torsion). Five full-scale fixed-fixed specimens were tested to study the effects of torsion to shear-depth ratio (T/Vd) and the bottom longitudinal tensile reinforcement ratio (ρ_l). Furthermore, a three-dimensional finite element model (FEM) was developed using ABAQUS software and verified against the experimental data. Finally, a parametric study was performed to assess the influences of transverse reinforcement ratio (ρ_t) and wall thickness to width ratio (t_w/b). The following findings are introduced in light of the used dimensions, parameters, and presented discussions:

1. The failure mode of the SCRC box girders tested under combined loading is significantly affected by the longitudinal tensile reinforcement ratio (ρ_l) and the transverse reinforcement ratio (ρ_t). At conditions where $\rho_l < 2.67$ % or $\rho_t \geq 0.67$%, kept the other parameters constant, the failure mode shifted to flexural failure characterized by the yielding of the bottom longitudinal tensile reinforcement, in contrast to the transverse reinforcement.
2. Increasing the T/Vd ratio of SCRC box girders from 0.18 % to 0.92 %, while maintaining the same longitudinal tensile reinforcement ratio, led to a nearly 40.7 % reduction in the ultimate load along with a decrease in ultimate mid-span deflection by about 67.6 %. This may be attributed to the spreading and widening of excessive diagonal cracks when the torsional moment increases, which in turn led to a decline in energy absorption.
3. The longitudinal tensile reinforcement ratio was directly proportionate to the capacity of the tested SCRC box girders. The ultimate load of specimen BG-0.64–4.20–0.25–0.21 (244.9 kN) was about 60.2 % higher than that of specimen BG-0.64–1.29–0.25–0.21 (152.9 kN). In contrast, the energy absorption for the former was about 63.2 % lower than that for the latter.
4. Up to the transverse reinforcement ratio of 1.05 %, it was evident that every increase in this ratio corresponded with an increase in the ultimate capacity of the tested SCRC box girders. However, beyond this ratio, the increase in capacity diminished due to the occurrence of concrete crushing before the steel yielding. Additionally, specimen BG-0.64–3.24–1.05–0.21 demonstrated superior energy absorption compared to specimen BG-0.64–3.24–0.19–0.21, with a value of 7545 kN.mm, an increase of almost 60.1 %.
5. Doubling the wall thickness to width ratio at T/Vd of 0.64 resulted in an increase in the ultimate load and the corresponding ultimate deflection by approximately 26.0 % and 43.7 %, respectively. Besides, during the post-peak stage, a sudden drop in the ultimate load was nearly avoided in all specimens with higher wall thickness to width ratios, indicating an improvement in their energy absorption. This enhancement is attributed solely to the extra-contribution of concrete webs, rather than the transverse reinforcement.
6. It should be noted that these findings are only limited to the tested SCRC box girders, and further refinement will be attained through additional experimental work.
7. Future experimental and numerical studies are needed to extend this analysis to evaluate the thermomechanical behavior of SCRC box girders under elevated temperatures or standard fire conditions. Contributing to the provision of a valuable database that will open up new research opportunities, allowing future work to extend the analysis beyond existing test cases.

CRediT authorship contribution statement

Tarek F. El-Shafiey: Supervision, Conceptualization. **Emad E. Etman:** Supervision, Conceptualization. **Ahmed M. Atta:** Supervision, Conceptualization. **Asmaa F. Edris:** Writing – review & editing, Writing – original draft, Resources, Formal analysis, Data curation. **Ahmed T. Baraghith:** Writing – review & editing, Writing – original draft, Resources, Methodology, Investigation, Formal analysis, Data curation, Conceptualization.

Funding

The author(s) received no financial support for the research, authorship, and/or publication of this article.

Conflict of Interest

The author(s) declared no potential conflicts of interest with respect to the research, authorship, and/or publication of this article.

References

[1] MohamedSalih MM, Yousif AR. Effect of reinforcement type on the behavior of rectangular HSC box-girders under combined torsion-shear-flexure: an experimental study. Structures, 37. Elsevier; 2022. p. 536–50. https://doi.org/10.1016/j.istruc.2022.01.029.
[2] Eltaly BA, Shaheen YB, Tayeh B, Henish AA. Enhancing the behavior of reinforced concrete box girders under two-point Loading: numerical and experimental investigations. Structures, 52. Elsevier; 2023. p. 386–400. https://doi.org/10.1016/j.istruc.2023.03.182.
[3] Gouda LP. Study on parametric behavior of single cell box girder under different radius of curvature (MSc. Thesis). India: National Institute of Technology Rourkela Odisha; 2013.
[4] Gupta PK, Singh KK, Mishra A. Parametric study on behavior of box girder bridges using finite element method. Asian J Civ Eng (Build Hous) 2010;11:135–48.
[5] Hemzah SA, Alyhya WS, Hassan SA. Experimental investigation for structural behaviour of self-compacting reinforced concrete hollow beams with in-place circular openings strengthened with CFRP laminates. Structures, 24. Elsevier; 2020. p. 99–106. https://doi.org/10.1016/j.istruc.2020.01.008.
[6] Revilla-Cuesta V, Ortega-López V, Skaf M, Khan AU, Manso JM. Deformational behavior of self-compacting concrete containing recycled aggregate, slag cement and green powders under compression and bending: description and prediction adjustment. J Build Eng 2022;15(54):104611. https://doi.org/10.1016/j.jobe.2022.104611.
[7] Mahmod M, Hanoon AN, Abed HJ. Flexural behavior of self-compacting concrete beams strengthened with steel fiber reinforcement. J Build Eng 2018;1(16):228–37. https://doi.org/10.1016/j.jobe.2018.01.006.
[8] Cattaneo S, Mola F. Assessing the quality control of self-consolidating concrete properties. J Constr Eng Manag 2012;138(2):197–205. https://doi.org/10.1061/(asce)co. 1943-7862.0000410.
[9] Hassan AA, Hossain KM, Lachemi M. Strength, cracking and deflection performance of large-scale self-consolidating concrete beams subjected to shear failure. Eng Struct 2010;32(5):1262–71. https://doi.org/10.1016/j.engstruct.2010.01.002.

[10] Shi C, Wu Z, Lv K, Wu L. A review on mixture design methods for self-compacting concrete. Constr Build Mater 2015;1(84):387–98. https://doi.org/10.1016/j.conbuildmat.2015.03.079.
[11] Tichko S, De Schutter G, Troch P, Vierendeels J, Verhoeven R, Lesage K, Cauberg N. Influence of the viscosity of self-compacting concrete and the presence of rebars on the formwork pressure while filling bottom-up. Eng Struct 2015;15(101):698–714. https://doi.org/10.1016/j.engstruct.2015.08.008.
[12] Domone PL. A review of the hardened mechanical properties of self-compacting concrete. Cem Concr Compos 2007;29(1):1–2. https://doi.org/10.1016/j.cemconcomp.2006.07.010.
[13] Vijayakumar A, Madhavi TC. Behaviour of self compacting concrete with hybrid fibers in hollow beams. Mater Today Proc 2021;1(46):3212–9. https://doi.org/10.1016/j.matpr.2020.11.193.
[14] Anuradha V, Madhavi TC. Behaviour of self compacting concrete hybrid fiber reinforced hollow beams. Structures, 35. Elsevier; 2022. p. 990–1001. https://doi.org/10.1016/j.istruc.2021.11.058.
[15] Devi K, Aggarwal P, Saini B. Admixtures used in self-compacting concrete: a review. Iran J Sci TechnolTrans Civ Eng 2020;44(2):377–403. https://doi.org/10.1007/s40996-019-00244-4.
[16] Imran M, Shafiq N, Akbar I. A review of combined flexure, shear & torsion strengthening of reinforced concrete beam. Annu Int Conf Archit Civ Eng 2013. https://doi.org/10.5176/2301-394x_ace13.147.
[17] Lopes SM, Bernardo LF. Cracking and failure mode in HSC hollow beams under torsion. Constr Build Mater 2014;31(51):163–78. https://doi.org/10.1016/j.conbuildmat.2013.10.062.
[18] Wang P, Huang Z. A unified approach for determining the ultimate strength of RC members subjected to combined axial force, bending, shear and torsion. Plos One 2017;17(12):e0175834. https://doi.org/10.1371/journal.pone.0175834.
[19] Yu Z, Shan D. Experimental and numerical studies of T-shaped reinforced concrete members subjected to combined compression-bending-shear-torsion. Adv Struct Eng 2021;24(12):2809–25. https://doi.org/10.1177/13694332211012577.
[20] Ren Y, Guo R, Liu A, Xia M, Pan Y. Study on flexural behaviour and analytical model of RC beams strengthened with FRP grid-ECC composite layers. Structures, 73. Elsevier; 2025, 108445. https://doi.org/10.1016/j.istruc.2025.108445.
[21] Yang W, Xu X, Zhang Z, Liu D, Hu H, Getahun D. Composite using ECC-steel wire to strengthen RC beams: flexural performance and FEM analysis. Case Stud Constr Mater 2025;22:e04286. https://doi.org/10.1016/j.cscm.2025.e04286.
[22] Yoo DY, Chun B, Choi J, Min KH, Shin HO. Enhancing the flexural capacity of RC beams under various loading rates through strengthening with ultra-high-performance fiber-reinforced concrete. Dev Built Environ 2024;20:100581. https://doi.org/10.1016/j.dibe.2024.100581.
[23] Codina A, Torres L, D'Antino T, Baena M, Barris C. Flexural performance of RC beams strengthened with HB CFRP plates: experimental study and theoretical model based on the intermediate crack debonding. Constr Build Mater 2025 2025; 458:139444. https://doi.org/10.1016/j.conbuildmat.2024.139444.
[24] Abadel AA. Flexural behaviour of RC beams with a UHPFRC top layer and hybrid reinforcement of steel and glass fiber reinforced polymer bars. Case Stud Constr Mater 2024;1(21):e04017. https://doi.org/10.1016/j.cscm.2024.e04017.
[25] Wang Y, Zheng H, Chen H, Chen Z, Zhuang N. Experimental and numerical study on the flexural properties of RC beams with different CFRP-strengthened schemes. J Build Eng 2024;97:110734. https://doi.org/10.1016/j.jobe.2024.110734.
[26] Ellithy M, Hassan A, El-Shafiey TF. Flexural strengthening of RC beams using PGFRP bars embedded in strain-hardening cementitious composites (SHCC). Eng Struct 2024;15(317):118628. https://doi.org/10.1016/j.engstruct.2024.118628.
[27] Afefy HM, Heniegal AM, Baraghith AT, Ibrahim OM, Eldwiny ME. Flexural behavior of RC continuous beams strengthened by cementitious composite materials. Civ Eng J 2024;10(9):2839–58. https://doi.org/10.28991/cej-2024-010-09-05.
[28] Khaled E, Hassan A, Mahmoud MH, El-Shafiey TF. Flexural behaviour of reinforced concrete slabs strengthened with textile-reinforced strain-hardening cementitious composites subjected to post-strengthening corrosion. Eng Struct 2025;15(329): 119822. https://doi.org/10.1016/j.engstruct.2025.119822.
[29] Khalil AE, Atta AM, Hassan A, Abd-Elaaty AH. Flexural strength recovery of RC one-way slabs having cut-outs using NSM-SHCC plates. Eng Struct 2022;1(258): 114149. https://doi.org/10.1016/j.engstruct.2022.114149.
[30] Mansour W, Ebead U, Nagib MT, Fayed S. Behavior of hollow self-compacted concrete beams reinforced with aluminum sections. Structures, 52. Elsevier; 2023. p. 549–67. https://doi.org/10.1016/j.istruc.2023.04.013.
[31] Jin L, Qin P, Zhang J, Li D, Jiang XA, Du X. Size effect in shear failure of RC beams reinforced with CFRP sheets: influences of CFRP adhesion angle and shear-span ratio. Eng Struct 2025;1(326):119543. https://doi.org/10.1016/j.engstruct.2024.119543.
[32] Bui LV. Developed method for analyzing maximum shear capacity of RC beams retrofitted with embedded through-section FRP reinforcement. Structures, 71. Elsevier; 2025, 108123. https://doi.org/10.1016/j.istruc.2024.108123.
[33] Jiang C, Xiong W, Fu Y, Ye J. Experimental investigation on shear performance of RC T-beams strengthened with hybrid bonded CFRP strips. Eng Fail Anal 2025;167: 109080. https://doi.org/10.1016/j.engfailanal.2024.109080.
[34] Zhou J, Wang X, Ding L, Tao J, Liang X, Wu Z. Evaluation of the shear behavior of RC beams strengthened with prestressing BFRP grids. Constr Build Mater 2024; 452:138978. https://doi.org/10.2139/ssrn.4839804.
[35] You X, Wang P, Shi Q, Rong C. Study on the influence of section dimensions on the shear performance of RC beam with UHPC formwork. Structures, 68. Elsevier; 2024, 107221. https://doi.org/10.1016/j.istruc.2024.107221.
[36] Abdullah M, Nakamura H, Miura T. Experimental investigation on influence of vertical stirrup legs to shear failure behavior in RC beams. Dev Built Environ 2024; 18:100451. https://doi.org/10.1016/j.dibe.2024.100451.
[37] Kannam P, Sarella VR. A study on validation of shear behaviour of steel fibrous SCC based on numerical modelling (ATENA. J Build Eng 2018;19:69–79. https://doi.org/10.1016/j.jobe.2018.05.003.
[38] Etman EE, Afefy HM, Baraghith AT, Khedr SA. Improving the shear performance of reinforced concrete beams made of recycled coarse aggregate. Constr Build Mater 2018;10(185):310–24. https://doi.org/10.1016/j.conbuildmat.2018.07.065.
[39] Etman EE, Afefy HM, Baraghith AT, Abuelwafa M. Shear behavior of RC beams reinforced with internal trussed steel strips at shear span zone. Structures, 32. Elsevier; 2021. p. 1734–51. https://doi.org/10.1016/j.istruc.2021.03.093.
[40] Khalil AE, Atta AM, Baraghith AT, Behiry RN, Soliman OE. Shear strengthening of concrete deep beams using pre-fabricated strain-hardening cementitious composite plates. Eng Struct 2023;1(278):115548. https://doi.org/10.1016/j.engstruct.2022.115548.
[41] Zhou C, Wang J, Shao X, Li L, Qiu M. Enhancing torsional behavior of RC beams: the potential of ultra-high performance concrete (UHPC. Compos Struc 2025;1 (357):118950. https://doi.org/10.1016/j.compstruct.2025.118950.
[42] Mane VV, Patil NK. A study on torsional behaviour of rectangular reinforced concrete beams with U-shaped encased welded wire mesh. Mater Today Proc2023 . https://doi.org/10.1016/j.matpr.2023.05.570.
[43] Gasir H, Khalil MM, Elsalakawy TS, Mustafa TS. Torsional performance of rubberized concrete beams containing steel fibers and steel tiers. Structures, 77. Elsevier; 2025, 109118. https://doi.org/10.1016/j.istruc.2025.109118.
[44] Elkhouly AF, Eltaly BA, Khalifa AE, Abdelmgeed FA. Torsional behavior of reinforced concrete stepped beams: an experimental and numerical investigation. Structures, 71. Elsevier; 2025, 108045. https://doi.org/10.1016/j.istruc.2024.108045.
[45] Zhang Z, Xie TY, Zhao XY. Torsional behavior of ultra-high-performance fiber-reinforced concrete beams: testing, modeling and design recommendation. J Build Eng 2025:113885. https://doi.org/10.1016/j.jobe.2025.113885.
[46] Lei Y, Li D, Jin L, Du X. Experimental study on torsional size effect of BFRP bars-RC beams. Eng Struct 2025;1(326):119595. https://doi.org/10.1016/j.engstruct.2024.119595.
[47] ELWakkad NY, Heiza KM, Mansour W. Experimental study and finite element modelling of the torsional behavior of self-compacting reinforced concrete (SCRC) beams strengthened by GFRP. Case Stud Constr Mater 2023;1(18):e02123. https://doi.org/10.1016/j.cscm.2023.e02123.
[48] Atta AM, El-Shafiey TF. Strengthening of RC dapped-end beams under torsional moment. Mag Concr Res 2014;66(20):1065–72. https://doi.org/10.1680/macr.14.00067.
[49] ACI Committee. Building code requirements for structural concrete (ACI 318-25) and commentary. Farmington Hills, MI: American Concrete Institute; 2025. p. 519.
[50] ECP 203. Egyptian Code of Practice for Design and Construction of Reinforced Concrete Structures. Hous Build Natl Res Cent Egypt 2020.
[51] CSA A23.3:19, 2019. Design of Concrete Structures. Mississauga, ON, Canada: Canadian Standards Association.
[52] American Association of Highway and Transportation Officials. 2017. AASHTO LRFD Bridge Design Specifications, 8th Edition, Washington, D.C.
[53] European Committee for Standardization. 2004. Eurocode 2: Design of concrete structures - Part 1-1: General rules and rules for buildings, Brussels, Belgium.
[54] Alnuaimi AS, Al-Jabri KS, Hago A. Comparison between solid and hollow reinforced concrete beams. Mater Struct 2008;41(2):269–86. https://doi.org/10.1617/s11527-007-9237-x.
[55] MohamedSalih MM, Yousif AR. Experimental study on torsional behavior of thin- and thick-walled RC box-girders using BFRP bars and steel stirrups under combined torsion-shear-moment. Structures, 36. Elsevier; 2022. p. 549–64. https://doi.org/10.1016/j.istruc.2021.12.031.
[56] Deifalla A, Awad A, Seleem H, Abdelrahman A. Experimental and numerical investigation of the behavior of LWFC L-girders under combined torsion. Structures, 26. Elsevier; 2020. p. 362–77. https://doi.org/10.1016/j.istruc.2020.03.070.
[57] Deifalla A, Awad A, Seleem H, Abdelrahman A. Investigating the behavior of lightweight foamed concrete T-beams under torsion, shear, and flexure. Eng Struct 2020;219:110741. https://doi.org/10.1016/j.engstruct.2020.110741.
[58] Hibbitt, K., 2000. Sorensen: ABAQUS Theory manual, Version 6.1. Pawtucket: Hibbitt, Karlsson and Sorensen.
[59] Ibrahim MS, Gebreyouhannes E, Muhdin A, Gebre A. Effect of concrete cover on the pure torsional behavior of reinforced concrete beams. Eng Struct 2020;216: 110790. https://doi.org/10.1016/j.engstruct.2020.110790.
[60] Xu J, Diao B, Guo Q, Ye Y, Mo YL, Zhou T. Parametric study on mixed torsional behavior of U-shaped thin-walled RC girders. Adv Civ Eng 2018;2018(1):3497390. https://doi.org/10.1155/2018/ 3497390.
[61] Lei Y, Jin L, Li D, Zhu H, Du X. Comparison of torsional damage and size effects of BFRP-and steel-reinforced concrete beams with different stirrup ratios. Eng Struct 2023;285:116042. https://doi.org/10.1016/j.engstruct.2023.116042.
[62] Lei Y, Jin L, Du X. Experimental investigation of size effects on BFRP-RC beams under combined bending-shear-torsion loading. Eng Struct 2025;336:120457. https://doi.org/10.1016/j.engstruct.2025.120457.
[63] Karimipour A, De Brito J, Ghalehnovi M, Gencel O. Torsional behaviour of rectangular high-performance fibre-reinforced concrete beams. Structures, 35. Elsevier; 2022. p. 511–9. https://doi.org/10.1016/j.istruc.2021.11.037.
[64] Said M, Salah A, Erfan A, Esam A. Experimental analysis of torsional behavior of hybrid fiber reinforced concrete beams. J Build Eng 2023;15(71):106574. https://doi.org/10.1016/j.jobe.2023.106574.

[65] Patane A, Vesmawala G. Experimental and analytical investigation of the behaviour of reinforced concrete beam under pure torsion. Mater Today Proc 2023. https://doi.org/10.1016/j.matpr.2023.03.539.
[66] Kaya SA, Yalçın C, Kaya O. Experimental investigation of full-scale reinforced concrete beams under reversed-cyclic pure torsion. Structures, 51. Elsevier; 2023. p. 734–46. https://doi.org/10.1016/j.istruc.2023.03.079.
[67] Zhou C, Wang J, Jia W, Fang Z. Torsional behavior of ultra-high performance concrete (UHPC) rectangular beams without steel reinforcement: experimental investigation and theoretical analysis. Compos Struct 2022;1(299):116022. https://doi.org/10.1016/j.compstruct.2022.116022.
[68] Liao Q, Su Y, Yu J, Yu K. Torsional behavior of BFRP bars reinforced engineered cementitious composites beams without stirrup. Eng Struct 2022;1(268):114748. https://doi.org/10.1016/j.engstruct.2022.114748.
[69] ASTM C31/C31M. "Standard practice for making and curing concrete test specimens in the field". West Conshohocken, PA, USA: ASTM International; 2019. ⟨www.astm.org⟩.
[70] Nagataki S, Fujiwara H. Self-compacting property of highly flowable concrete. In: Malhotra VM, editor. Second Conference on Advances in Concrete Technology. ACI SP-154. American Concrete Institute; 1995. p. 301–14.
[71] Okamura H, Ozawa K. Mix design for self-compacting concrete. Concr Libr Jpn Soc Civ Eng 1995:107–20.
[72] ASTM C496/C496M-17. Standard test method for splitting tensile strength of cylindrical concrete specimens. Conshohocken, PA, USA: ASTM International; 2017. ⟨www.astm.org⟩.
[73] ASTM A615/A615M-16. Standard specification for deformed and plain carbon steel bars for concrete reinforcement. West Conshohocken, PA, USA: ASTM International; 2016. ⟨www.astm.org⟩.
[74] Fernandes B, Masiero Gil A, Longhi Bolina F, Fonseca Tutikian B. Thermal damage evaluation of full scale concrete columns exposed to high temperatures using scanning electron microscopy and X-ray diffraction. Dyna 2018;85(207):123–8. https://doi.org/10.15446/dyna.v85n207.70593.
[75] Bolina FL, Tutikian B, Rodrigues JP. Experimental analysis on the structural continuity effect in steel decking concrete slabs subjected to fire. Eng Struct 2021;1(240):112299. https://doi.org/10.1016/j.engstruct.2021.112299.
[76] Baraghith AT, Mansour W, Behiry RN, Fayed S. Effectiveness of SHCC strips reinforced with glass fiber textile mesh layers for shear strengthening of RC beams: experimental and numerical assessments. Constr Build Mater 2022;327:127036. https://doi.org/10.1016/j.conbuildmat.2022.127036.
[77] Atta AM, Behiry RN, Haraz MI. Effectiveness of external prestressing in enhancing the non-ductile hanger failure mechanism in reinforced concrete inverted T-beams. Front Struct Civ Eng 2024;18(7):1050–65. https://doi.org/10.1007/s11709-024-1026-x.
[78] Baraghith AT, Khalil AH, Etman EE, Behiry RN. Improving the shear behavior of RC dapped-end beams using precast strain-hardening cementitious composite (P-SHCC) plates. Structures, 50. Elsevier; 2023. p. 978–97. https://doi.org/10.1016/j.istruc.2023.02.059.
[79] Issa ME, El-Shafey NF, Baraghith AT, Balat EN. Flexural strengthening of LWRC beams using RSHCC reinforced with glass fiber textile mesh. J Eng Appl Sci 2024;71(1):132. https://doi.org/10.1186/s44147-024-00467-x.
[80] Afefy HM, Baraghith AT, Hassan A, Abuzaid MK. Strengthening of shear-deficient RC beams using near surface embedded precast cement-based composite plates (PCBCPs. Eng Struct 2021;244:112765. https://doi.org/10.1016/j.engstruct.2021.112765.
[81] Hillerborg A. The theoretical basis of a method to determine the fracture energy GF of concrete. Mater Struct 1985:291–6. https://doi.org/10.1007/bf02472919.
[82] Park R, Paulay T. Reinforced concrete structures. John Wiley & Sons; 1991.